DRAFT

Stiffness, Strength, and Performance of Unbound Aggregate Material: Application of South African HVS and Laboratory Results to California Flexible Pavements

Report produced under the auspices of the California Partnered Pavement Research Program

by:

H L Theyse
CSIR Transportek
PO Box 395
Pretoria, Republic of South Africa
0001

University of California
Pavement Research Center
July 2002

TABLE OF CONTENTS

LIST OF FIGURES

LIST OF TABLES

1.0 INTRODUCTION

Caltrans specifies the use of a 75-mm Asphalt Treated Permeable Base (ATPB) layer as standard practice for all new flexible pavement designs in California.(*1*) The ATPB acts as a drainage layer beneath the asphalt concrete (AC) and is supported by an aggregate base layer. However, the potential exists for water to enter the unbound aggregate base layer from the ATPB layer through the prime coat that separates them. The stiffness, strength, and performance of unbound aggregate layers are largely influenced by moisture content.

The assessment of the performance of two types of flexible pavement cross section, one with and one without an ATPB layer, were included in the strategic plan of the CAL/APT program (1994–2000). Goal 1 and Goal 5 of the CAL/APT project (continued in the Partnered Pavement Research Program after 2000) consist of the evaluation of these two sections under dry and wet base conditions, respectively.

The evaluation includes accelerated pavement testing using the Heavy Vehicle Simulator (HVS) and laboratory testing. The test plan for Goal 5 (*2*) includes, "the evaluation of the effects of compaction and water content on the stiffness of the aggregate base and subbase layers." The first objective of Goal 5 is to measure the effectiveness of the ATPB layer in the drained pavement in preventing a decrease in stiffness and strength of the unbound layers. Those results are included in References (*3*–*6*). It is, however, not only the degree of saturation of an unbound aggregate that influences the performance of the material but also the level of compaction of the material.

The objective of this report is to illustrate the effect of the level of compaction and the degree of saturation on the stiffness, strength, and plastic deformation of unbound aggregate layers based on information obtained from HVS and laboratory testing in South Africa. The results will permit extrapolation of Goal 1 and Goal 5 results to other California materials and

structures. The information presented in this report also contributes towards the improved understanding and modeling of the behavior of unbound aggregate material for mechanistic-empirical design purposes.

The scope of the information presented herein is limited to the aggregate used for pavement base and subbase layers. A comparison of California and South Africa specifications for base and subbase aggregate material is presented to identify possible similar material categories for which it is thought similar response and behavior will be exhibited.

HVS tests that were performed on pavements with unbound aggregate base layers were identified and the deflection and permanent deformation responses of these test sections were extracted from the CSIR HVS database to be evaluated in terms of the objective of this report. Data from laboratory projects that were performed in association with the HVS program in South Africa in addition to the HVS data are presented in order to facilitate a more detailed evaluation of the effect of density and degree of saturation on the stiffness, strength, and plastic deformation of unbound aggregate material.

2.0 CALIFORNIA AND SOUTH AFRICA AGGREGATE

The California and South Africa materials classification systems distinguish between different aggregate classes or categories. In the case of the California material specification, a distinction is made between aggregates for base and subbase layers. Three subbase aggregate classes, ranging from Class 1 to Class 3, and two base aggregate classes, Class 2 and Class 3 aggregate, are defined. The definitions of these material classes are based on the gradation, a shear resistance value (R-value), and sand equivalent value. Aggregate base materials also have an additional durability specification.

The South Africa material classification system (*7*) places more emphasis on the source of the aggregate than the layer in which it is used. A range of material categories is defined for unbound pavement materials ranging from high quality crushed stone (G1 and G2) to in-situ subgrade quality material (G10). These material classes are defined according to criteria for gradation (gradation envelopes and a gradation modulus), Atterberg limits, bearing strength (CBR), resistance to abrasion, and density requirements for different applications. Base and subbase quality aggregate will typically fall in the upper material categories ranging from G1 to G3 for processed crushed stone material and G4 to G6 for natural gravels.

Ideally, the comparison between the California and South Africa materials specifications needs to be based on at least the following:

- Gradation requirements
- Activity (swell, plasticity, clay content, sand equivalent or any similar method of quantification)
- Bearing strength (CBR or R-value)
- Density specifications

Unfortunately, the methods for determining the activity and bearing strength differ between California and South Africa, which effectively reduces the basis for the comparison to the gradation and density specification. A more detailed comparison may be possible if correlations between CBR and R-value, and Sand Equivalent and Atterberg limits can be established from the literature.

2.1 California Specification

2.1.1 Source of the Material

The aggregate for Class 2 and 3 aggregate base layers must be free from organic matter and deleterious substances. The aggregate may contain material from reclaimed asphalt concrete, portland cement concrete, lean concrete, cement treated base, or a combination of any of these materials as long as the volume of the reclaimed material does not exceed 50 percent of the total volume of the aggregate. The specification is not clear on the source for the other 50 percent of the aggregate, but it is assumed that it will be obtained from the crushing of rock or natural gravel. The same criteria apply to the aggregate for subbase layers.

2.1.2 Gradation Requirements

The California gradation requirement for base and subbase aggregate is given in Tables 1 and 2, respectively. The gradation for Class 3 base aggregate must comply with the gradation of either the 37.5- or 19.0-mm Class 2 aggregate or the gradation specified under special provisions. There is no specification requirement for fractured particles.

Table 1 Gradation Specification for Base Layer Aggregate

Sieve size (mm)	Maximum Nominal Size (mm)			
	37.5		19.0	
	Operating Range	Contract Compliance	Operating Range	Contract Compliance
50.0	100	100	–	–
37.5	90–100	87–100	–	–
25.0	–	–	100	100
19.0	50–85	45–90	90–100	87–100
4.75	25–45	20–50	35–60	30–65
0.600	10–25	6–29	10–30	5–35
0.075	2–9	0–12	2–9	0–12

Table 2 Gradation Specification for Subbase Layer Aggregate

Sieve size (mm)	Aggregate Class					
	Class 1		Class 2		Class 3	
	Operating Range	Contract Compliance	Operating Range	Contract Compliance	Operating Range	Contract Compliance
75.0	100	100	100	100	100	100
63.0	90–100	87–100	90–100	87–100	90–100	87–100
4.75	35–70	35–70	40–90	35–95	50–100	45–100
0.075	0–20	0–23	0–25	0–29	0–30	0–34

2.1.3 Quality Requirements

The material quality requirements for base and subbase aggregate are set out in Tables 3 and 4, respectively. The California density specification for unbound aggregate requires a minimum relative density of 95 percent of the maximum wet density achieved in the laboratory according to California Test Method No. 216 (CTM 216). For some aggregate materials, the maximum density obtained with CTM 216 is similar to that obtained with the AASHTO T-180 test method. AASHTO test T-180 is also referred to as the *modified AASHTO* test in this report.

Table 3 Quality Requirements for Base Layer Aggregate

Test Parameter	Operating Range	Contract Compliance Minimum Value
Resistance (R-value)	-	78
Sand Equivalent	25 minimum	22
Durability Index	-	35

Table 4 Quality Requirements for Subbase Layer Aggregate

Test Parameter	Aggregate Class					
	Class 1		Class 2		Class 3	
	Operating Range	Contract Compliance	Operating Range	Contract Compliance	Operating Range	Contract Compliance
Sand Equivalent	21 min	18 min	21 min	18 min	21 min	18 min
Resistance (R-value)	–	60 min	–	50 min	–	40 min

2.2 South Africa Specification

2.2.1 Source of the Material

The South Africa material specification for base and subbase aggregate places more emphasis on the source from which the aggregate is obtained and the way in which the aggregate is processed. Distinction is made between the crushed stone used for the construction of a G1 high density layer, the crushed stone used for a G2 or G3 layer, and aggregate from a natural gravel source.

2.2.1.1 Graded crushed stone G1

The material for a G1 crushed stone aggregate is obtained from crushing solid, unweathered rock. All the faces of the aggregate particles will therefore be fractured. The gradation of the material may only be adjusted by adding fines produced from the crushing of the original parent rock.

2.2.1.2 Graded crushed stone G2 and G3

The material for a G2 and G3 aggregate is obtained from crushing rock, boulders, or coarse gravel. At least 50 percent by mass of the individual fractions in excess of 4.75 mm should have at least one fractured face. The crushed material may include natural fines from sources other than from crushing of the parent rock.

2.2.1.3 Crushed stone and natural gravel G4, G5, and G6

G4, G5, and G6 quality aggregate may be obtained from natural gravel and boulders that may require crushing. The classification of the material as being G4, G5, or G6 is determined by the soaked CBR of the material. Normally, a G5 and G6 material will be used in subbase layers and a G4 material in base layers. The plasticity index (PI) may be adjusted by the addition of small quantities of lime, cement, or sand. All material passes the 63-mm sieve.

2.2.2 Gradation Requirements

The gradation requirement for a base layer aggregate is given in Table 5. Only a maximum particle size and gradation modulus specification is given for subbase aggregate (G5 and G6) (see Table 6).

Table 5 Gradation Requirements for Base Layer Aggregate

Sieve size (mm)	**Percentage Passing by Mass**		
	Material Type		
	G1, G2 and G3 Nominal Maximum Size of Aggregate (mm)		**G4**
	37.5	**26.5**	
53.0	100	100	100
37.5	100	100	85 – 100
26.5	84–94	100	-
19.0	71–84	85–95	60–90
13.2	59–75	71–84	-
4.75	36–53	42–60	30–65
2.00	23–40	27–45	20–50
0.425	11–24	13–27	10–30
0.075	4–12	5–12	5–15

Table 6 Quality Requirement for Base Aggregate

Property		Material Type	
		G1	G2, G3 and G4
Minimum CBR (%) at 98 % mod. AASHTO compaction		-	80
Maximum swell (%) at 100 % mod. AASHTO compaction		-	0.2
Crushing strength:	Minimum 10 % FACT[†] (kN)	110	110 (G2)[*]
	Maximum ACV[‡] (%)	29	29 (G2)[*]
Maximum Flakiness Index (%)[§]		35	35
Atterberg limits:	maximum Liquid Limit (LL)[**]	25	25
	maximum Plasticity Index (PI) [††]	4	6
	maximum Linear Shrinkage, % (LS) [‡‡]	4	3
Minimum compaction requirements:	i) % Apparent Density	86 - 88	-
	ii) % mod. AASHTO compaction		100 – 102 (G2) 98 (G3, G4)

[*] Only applicable to G2 material, not G3 and G4 material.

[†] 10% FACT (Fines Aggregate Crushing Value) is the the force in kN required to crush a sample of aggregate passing the 13.2 mm and retained on the 9.5 mm sieve so that 10 percent of the total test sample will pass a 2.36 mm sieve.

[‡] The aggregate crushing value (ACV) of an aggregate is the mass of material, expressed as a percentage of the test sample which is crushed finer than a 2.36 mm sieve when a sample of aggregate passing the 13.2 mm and retained on the 9.50 mm sieve is subjected to crushing under a gradually applied compressive load of 400 kN.

[§] Flakiness Index is a measure of the length to width ratio of aggregate particles

[**] Liquid Limit is the moisture content of a soil expressed as a percentage of mass of the oven-dried soil, at the boundary between the liquid and plastic states. The moisture content at this boundary is arbitrarily defined as the liquid limit and is the moisture content at a consistency determined by means of the standard liquid limit apparatus.

[††] Plasticity Index is the numerical difference between the liquid limit and the plastic limit of the soil and indicates the magnitude of the range of moisture contents over which the soil is in a plastic condition.

[‡‡] The linear shrinkage of a soil for the moisture content equivalent to the liquid limit, is the decrease in one dimension, expressed as a percentage of the original dimension of the soil mass, when the moisture content is reduced from the liquid limit to an oven-dry state.

2.2.3 Quality requirement

The quality requirement for base aggregate is given in Table 6; that of subbase aggregate is given in Table 7. The reference density for G1 aggregate is the apparent density of the course and fine fractions combined; 86 to 88 percent of apparent density is equivalent to about 106 to 108 percent of maximum dry density (MDD) determined according to the modified AASHTO (T-180) method.

Table 7 Quality Requirement for Subbase Aggregate

Property		Material Type	
		G5	G6
Minimum CBR (%) at: 95 % mod. AASHTO compaction 93 % mod. AASHTO compaction		45 -	- 25
Maximum swell (%) at 100 % mod. AASHTO compaction		0.5	1.0
Gradation requirement (maximum stone size)		63 mm or 2/3 of layer thickness	63 mm or 2/3 of layer thickness
Minimum gradation modulus		1.5	1.2
Atterberg limits:	maximum Liquid Limit (LL) maximum Plasticity Index (PI) maximum Linear Shrinkage, % (LS)	30 10 5	- 12 -
Min. Compaction requirements (% mod. AASHTO compaction)		95	95

2.3 Comparison of the California and South Africa Aggregate Specifications

2.3.1 Source of Material

The South Africa aggregate specification is more specific than the California specification in terms of the origin of crushed stone aggregate and how the individual particles are fractured, especially in the case of the South Africa specification G1 and G2 aggregates.

The California specification allows for a high percentage (up to 50 percent) of reclaimed material in the aggregate. The South Africa specification allows for the use of reclaimed pavement material as G4 to G6 material if the reclaimed material satisfies the specification for these material categories. No clear indication is given on the use of reclaimed pavement material for G1 to G3 material.

In the case of G1 material, the strict specification for this type of aggregate should rule out the use of reclaimed material. However, a material that was originally placed as a G1 may after years of service still comply with the specification for a G2 or G3 material and presumably may be used as such.

2.3.2 Gradation Requirement

Although not identical, the gradation requirement for the California Class 2 aggregate for base layers with a maximum size of 19 mm seems to be similar to the gradation requirement for a G2/G3 material with a 26.5-mm maximum particle size. This similarity in gradation envelope is illustrated in Figure 1. The colored solid squares in Figure 1 represent the control points for the gradation of a 19-mm maximum size crushed stone aggregate according to the California specification and the black lines represent the gradation envelope for a 26.5-mm maximum size aggregate according to the South Africa specification.

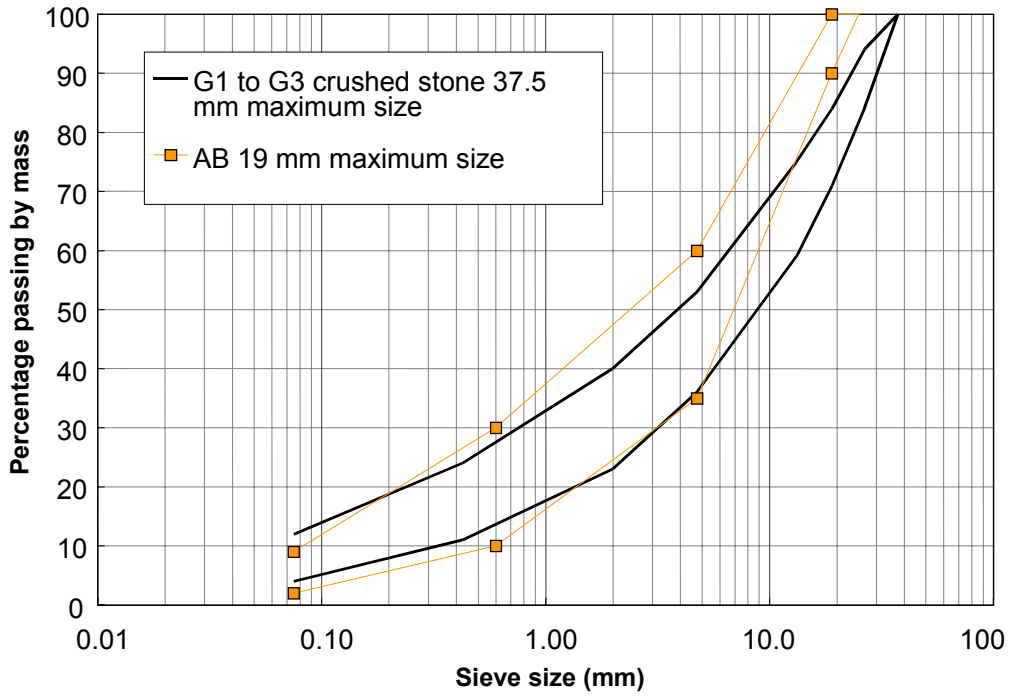

Figure 1. Comparison of the gradation envelopes for a 19-mm maximum size base layer aggregate from California and a 26.5-mm maximum size base layer aggregate from South Africa.

Figure 2a shows the dry gradation of three actual aggregate samples obtained from California base layers and sent to CSIR by the University of California Pavement Research Center, plotted with the South Africa gradation control points for a 26.5-mm maximum size crushed stone base layer aggregate as a reference. It is clear from this figure that the actual gradation of the California aggregate complies with the South Africa specification except for the larger particle sizes for which the actual gradation deviates slightly from the South Africa specification. Figure 2b shows the dry gradation of the three samples plotted with the control points for a dense aggregate gradation for a 19-mm maximum particle size material according to the Talbot equation. The Talbot equation estimates the gradation that will result in the maximum packing of particles for a given maximum aggregate size. It seems likely that the gradation of the California aggregate is based on the dense aggregate gradation for a 19-mm maximum particle size material.

Figure 3 shows the South Africa gradation envelope for a G4 aggregate and the California gradation control points for a Class 1 subbase aggregate plotted on the same graph. Although not exactly the same, there are similarities between the South Africa and California gradation specification. The South Africa specification limits the maximum particle size to 53 mm while the corresponding value for the California specification is 75 mm.

2.3.3 Quality Requirement

It is not possible to make a direct comparison between the quality criteria of California and South Africa aggregate as the parameters that are used to quantify the quality of the material differ between California and South Africa.

There are, however, two factors that largely influence the quality of compacted aggregate material: 1) the density levels to which the material is compacted, and 2) the moisture content of

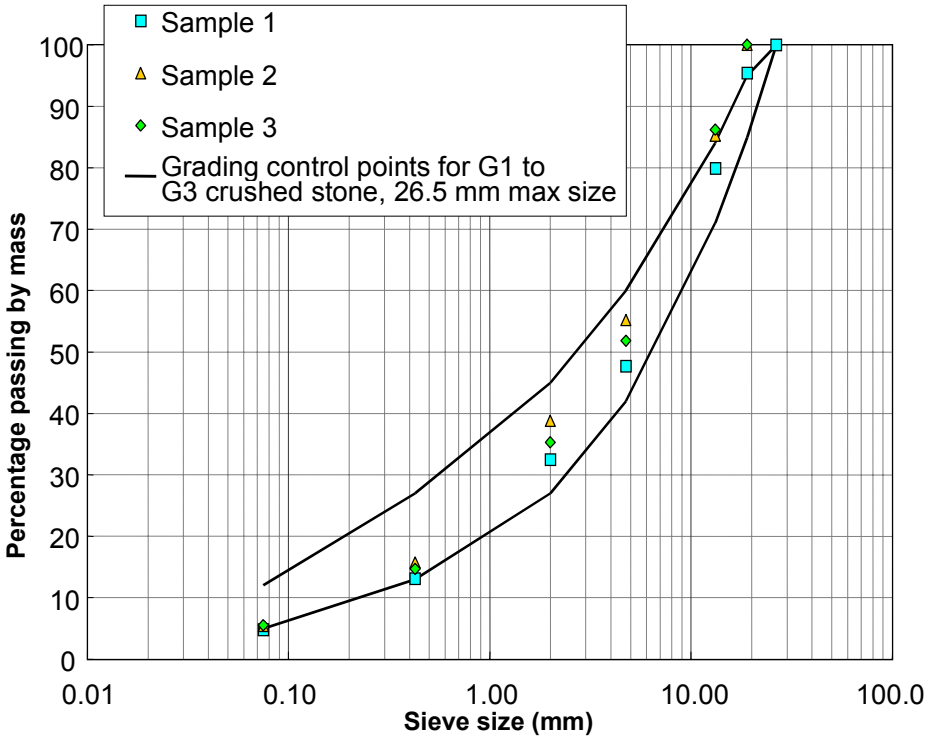

Figure 2a. Comparison of California samples with South Africa gradation control points for a 26.5-mm maximum particle size aggregate.

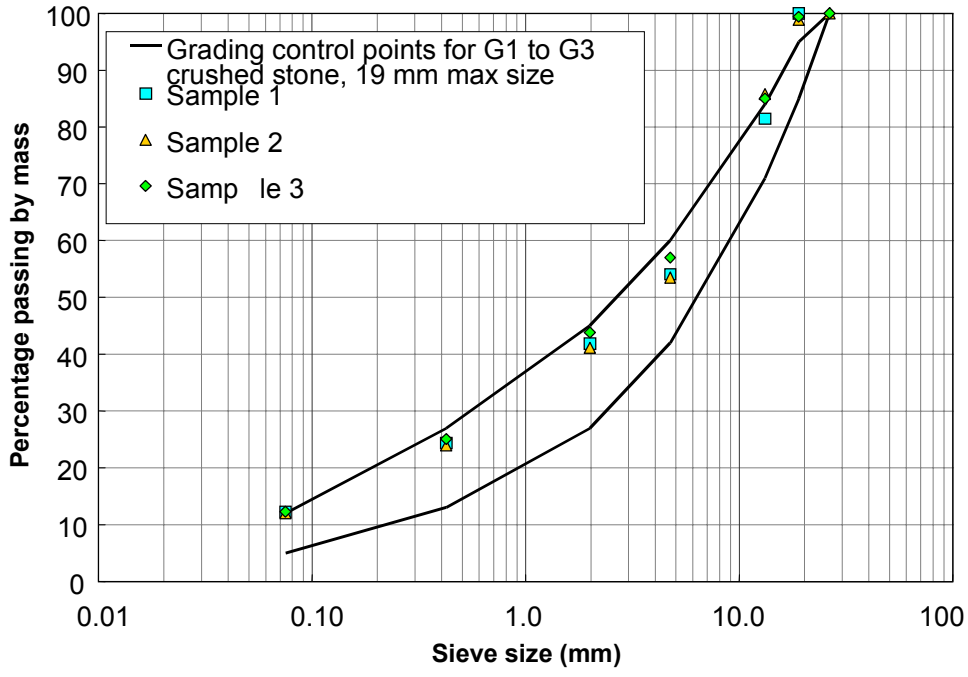

Figure 2b. Comparison of California samples with dense aggregate gradation control points for a 19-mm maximum particle size aggregate.

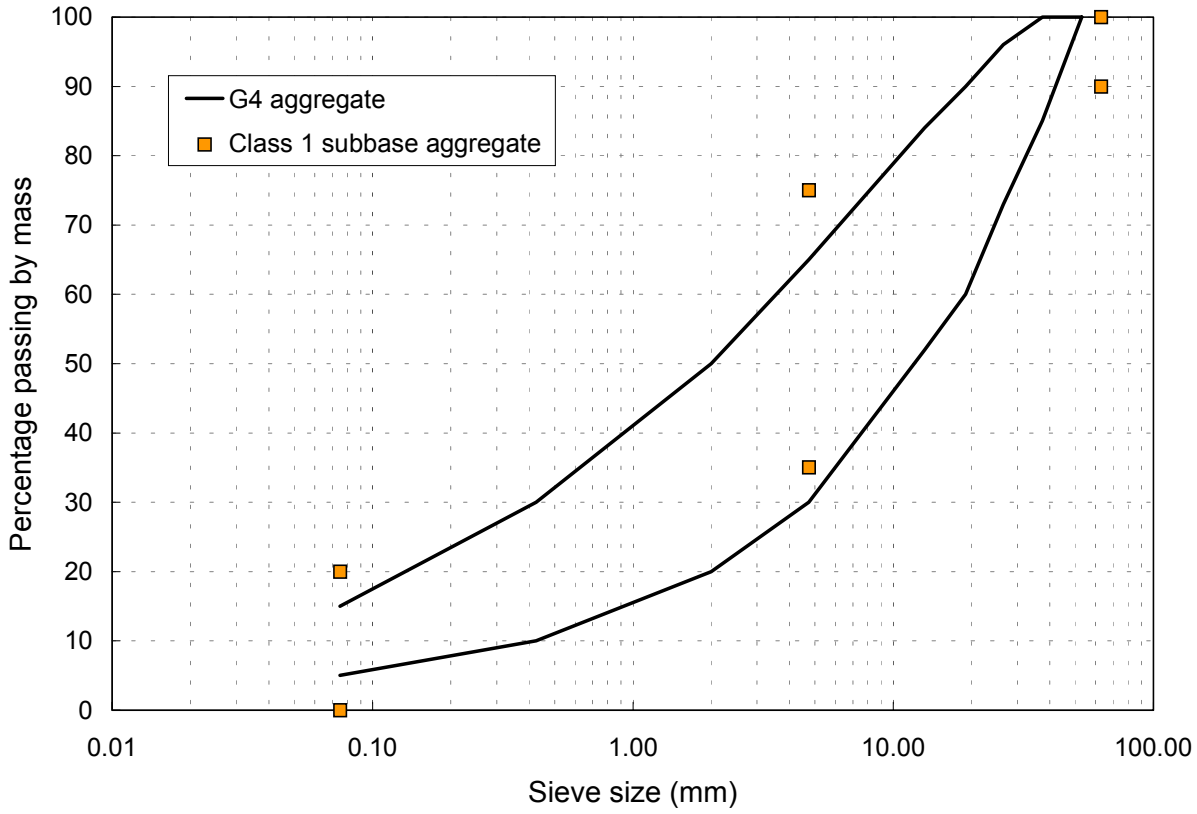

Figure 3. Comparison of the gradation envelopes for Class 1 subbase aggregate (California) and G4 aggregate (South Africa).

the material. As stated in the Introduction, the objective of this report is to illustrate the validity of this statement and to make this statement at this point is in a sense preempting the outcome of this study. The South Africa specification for aggregate material quality is, however, based on the principle that the density and moisture content of the material influences the quality of the compacted material. Therefore, in order to fully appreciate the South Africa material quality specification, it is necessary to provisionally accept this statement. Two examples of real data are included in this section of the report to substantiate this statement. Additional information on the effect of density and moisture content on the stiffness, strength, and plastic deformation of unbound aggregate are presented later in this report.

Figure 4 shows the CBR results for the three aggregate samples sent from California to CSIR compacted with the same amount of compaction energy at various moisture content levels. Although the density of the samples varied slightly, the effect that the relatively large variation in compaction moisture content had on the soaked CBR of the material overshadowed the effect that the relatively small variation in density had on the CBR.

Figure 5 shows the soaked CBR results of a number of samples of a G2 crushed stone aggregate from South Africa compacted with various compaction efforts. In this case the moisture content of the samples are about the same but the density varied and the effect of the density variation on the CBR of the material is clear.

The influence of density and moisture content on the quality (in the case of the examples, measured in terms of CBR) of the material is amply illustrated by the examples given in Figures 4 and 5. The influence of these parameters on the quality of the compacted material is incorporated in the South Africa specification for unbound aggregates. The minimum CBR for a specific aggregate category is given for a certain relative density under soaked moisture conditions. The minimum CBR for a G2, G3, and G4 classification is 80 percent at 98 percent of maximum dry density (MDD) determined according to the modified AASHTO (T-180) compaction method (see Table 6). The corresponding CBR values for a G5 and G6 classification are 45 and 25 percent at 95 and 93 percent relative density, respectively (see Table 7). All of these CBR values are soaked condition (4 days in a water bath) CBR values. The California specification for unbound aggregate does not specify a reference density and moisture content at which the R-value should be determined.

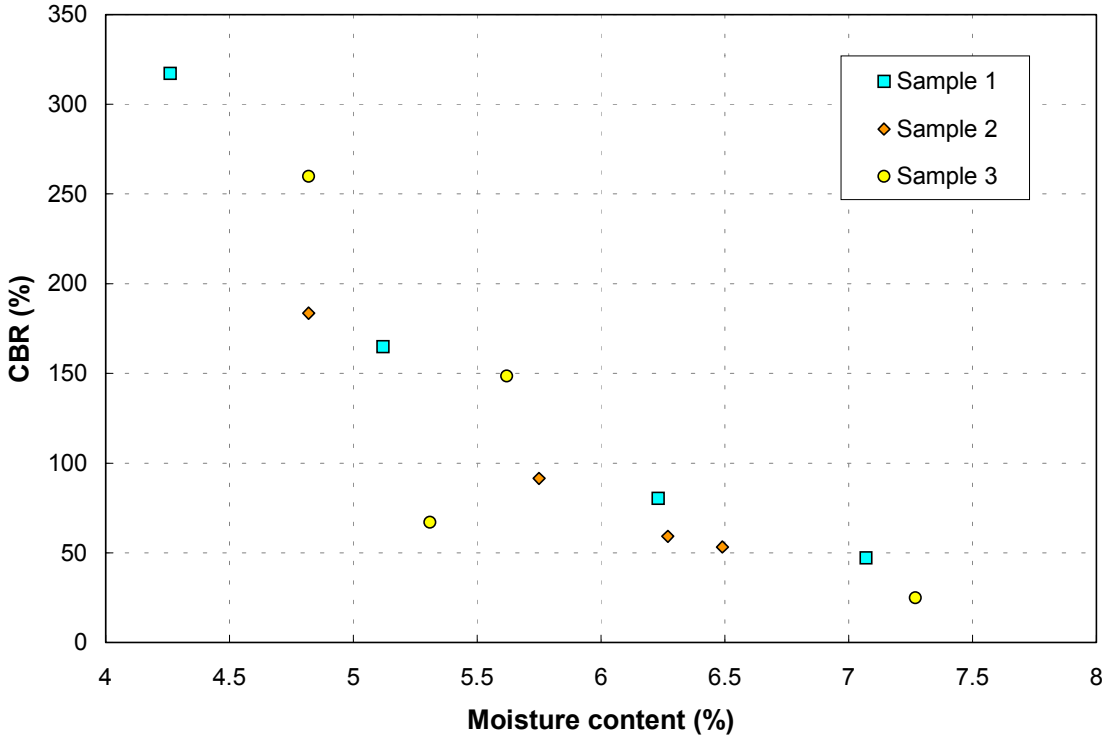

Figure 4. Combined CBR data for the three aggregates from California showing the relationship between compaction moisture content and CBR.

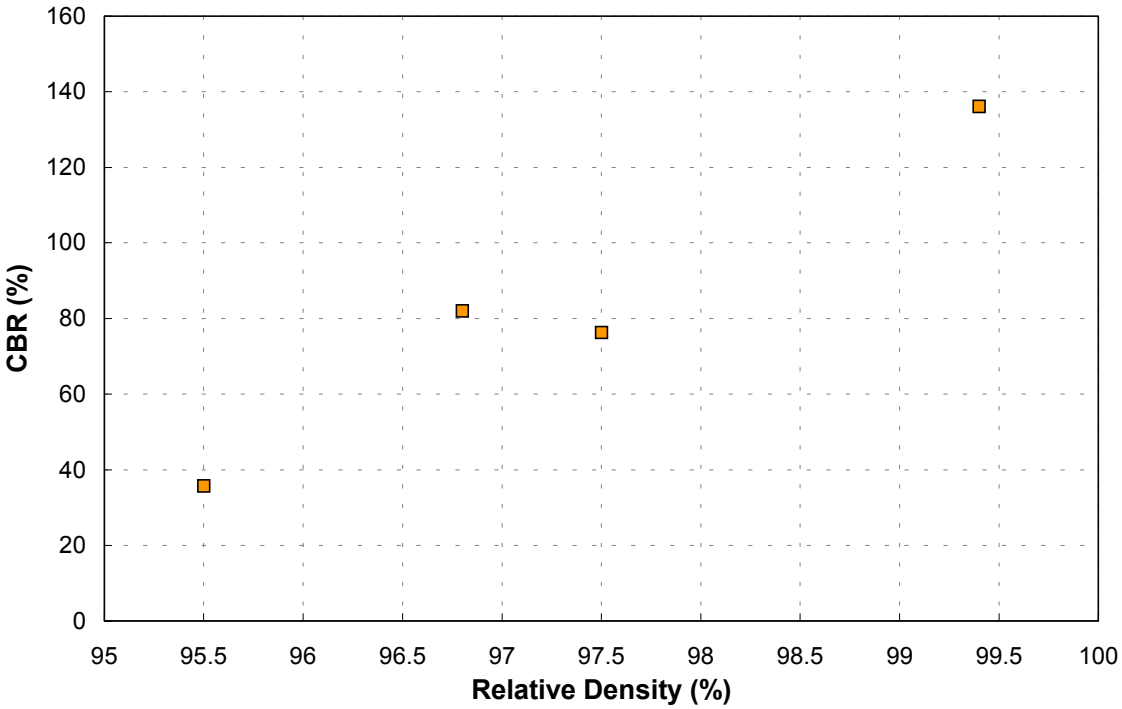

Figure 5. CBR data for a G2 aggregate from South Africa showing the relationship between compaction level and CBR.

Because of the large influence of density on the quality of the compacted aggregate, the South Africa specification requires certain minimum field compaction levels in terms of the reference density for various aggregate classes. The minimum requirement for a G1 material is 86 percent of apparent density, which is equivalent to approximately 106 to 108 percent of the modified AASHTO maximum dry density. The requirement for a G2 material is 100 percent of the modified AASHTO maximum dry density and that of G3 and G4 materials 98 percent of the modified AASHTO maximum dry density. For G5 and G6 material, the requirement is 95 percent of modified AASHTO maximum dry density.

The California specification requires field compaction to 95 percent of the reference density determined according to CTM 216. This reference density is, however, a wet density and not a dry density, as is the case for the South Africa specification. The maximum dry density obtained with CTM 216 is about approximately the same as the maximum dry density obtained with the modified AASHTO compaction method according to several comparisons performed at the University of California Pavement Research Center. If the material in the field is therefore at a moisture level above the optimum moisture content level for compaction, it will be possible to satisfy the specification in terms of wet density while the dry density may be below 95 percent of the dry maximum density.

In general, the field density requirement of the California specification is therefore much lower than that of the South Africa specification for aggregate base materials and similar for aggregate subbase materials.

To summarize, the following similarities and differences between California and South Africa aggregate are anticipated based on the comparison of the specifications for the two regions and limited data:

- **Source of material:** Although the California specification allows a large portion of recycled material in all aggregate classes, the basic material for both California and South Africa is obtained form crushed rock and boulders and natural gravel sources. Therefore, in terms of the source of the material and hence the nature of the material, California and South Africa aggregate are similar.
- **Gradation:** The gradation of a 19-mm maximum size Class 2 base aggregate in California seems to be similar to the gradation of 26.5-mm maximum size G2 and G3 aggregate in South Africa, except for some slight deviation at the larger particle sizes. The gradation specification for a Class 1 subbase aggregate seems similar to that of a G4 material. Therefore, in terms of gradation, there are similarities between certain classes of California and South Africa aggregate.
- **Quality of compacted material:** Although California and South Africa aggregate are similar in terms of the source of the material and the gradation of certain aggregate classes, the biggest difference between the aggregate for these two regions seems to be the specified field density for aggregate base materials. At this point, a direct comparison between the quality of the compacted aggregates is not possible because of differences in the way that the quality is measured. The large difference in specified field density between the California and South Africa specifications should result in a large difference in the quality or bearing strength of the placed material.

Comparison of the three California samples sent to CSIR and South Africa unbound aggregate indicates that they are similar in terms of the material consisting mostly of crushed stone or gravel particles with one or more broken faces and some agreement in the particle size

distribution, at least for specific material classes, although broken faces are not specified in California. The large differences between specified field densities for California and South Africa do not change the basic nature of the aggregate material, but will change the way the material responds to loading and long-term performance.

In addition to density, moisture content also has an influence on the behavior of unbound aggregate material. Data from Heavy Vehicle Simulator (HVS) and laboratory testing performed in South Africa prior to this study are used to illustrate the effect of the density and moisture content of an unbound aggregate material on the stiffness, strength and performance of the material. Because of the similarities between G2 and G4 material and certain California aggregate classes, the information presented in this document on the stiffness, strength, and plastic deformation of unbound aggregates is limited to these two South African material classes.

3.0 HVS STUDIES ON UNBOUND AGGREGATE BASE LAYERS

Several HVS tests have been performed in South Africa on pavements with unbound aggregate base layers consisting of crushed stone or natural gravel. The majority of these tests were performed on pavements with G2 crushed stone base layers and the results presented in this section of the report are largely from these HVS tests. The Multi-depth Deflectometer (MDD) system developed in South Africa and used extensively in association with the HVS provides the opportunity to study the resilient and plastic deformation response of pavement layers under HVS loading.

There are two requirements to enable a study of the resilient and plastic deformation of the pavement's layers from MDD data. First, the deflections at various depths below the surface should be recorded at various stages during the test to enable back-calculation of the effective stiffness of the layers. Second, the change in the offset of the MDD modules should be recorded at various stages during the test to enable calculation of the permanent displacement of the MDD modules. The permanent deformation of the pavement layers can then be calculated from the permanent MDD displacement data. The change in offset of the MDD modules was, however, only recorded from about the mid-1980s on CSIR test sections and therefore the plastic deformation data is only available for a limited number of HVS tests.

Part of the aim of this report is not only to investigate the stiffness, strength, and permanent deformation of unbound aggregate layers, but also to identify the factors affecting these parameters and to quantify the effect they have on the parameters that are investigated. There are three factors that determine the resilient and plastic response of unbound materials:

- the density of the compacted material,
- the moisture content of the compacted material, and

- the stress condition to which the material is subjected.

The deterioration of the material because of long-term traffic loading also causes a reduction in the stiffness of an unbound aggregate material. The results from a previous study conducted by Maree et al. (*8*) on the effect that the stress condition has on the stiffness of crushed stone and natural gravel aggregate is used to illustrate the effect of the stress condition on the stiffness of unbound aggregate. The depth deflection results from four HVS tests were utilized during Maree's study.

In addition to the Maree study, additional original work was performed for this report. Several HVS sections with crushed stone base layers for which the depth deflection and permanent MDD displacement data were available, were identified. The results from these HVS tests were used to investigate the stiffness and permanent deformation of unbound aggregate. Table 8 provides a summary of the HVS tests from which data was utilized in this report.

The one disadvantage of HVS testing compared to laboratory testing is that it is difficult to control the moisture content and density of the material that is being tested under the large-scale conditions of HVS testing. At best, the density and moisture content can be recorded during the test but this information is usually limited to a few points on the test section and only measured once or twice during the test, unless moisture content sensors are embedded in the test section. It therefore becomes difficult to investigate the effect of density and moisture content on the response of the pavement.

3.1 The effective stiffness response of unbound aggregate under HVS testing

Table 9 gives a summary of the back-calculated effective stiffness data from the study by Maree et al.(*8*) Table 10 contains a summary of the back-calculated effective stiffness data for

Table 8 HVS Tests from which Data Was Utilized in This Study

HVS Test No.	Road No.	Base Aggregate	Pavement Structure	Comments
42a4 – 45a4	Road P6/1	Natural gravel G5	40 mm asphalt concrete 200 mm G5 base 100 mm G8 subbase 200 mm G9 selected subgrade	Data from these test sections used by Maree et al. to illustrate the effect of stress condition on the effective stiffness of unbound aggregate.(*8*)
75a4 – 77a4	Road P123/1	Natural gravel G5	40 mm asphalt concrete 200 mm G5 base 150 mm G6 subbase 200 mm G8 selected subgrade	
101a4	Road P157/1	Crushed stone G2	30 mm asphalt concrete 200 mm G2 base 100 mm cemented subbase 200 mm G7 selected subgrade	
107a4	Road P157/2	Crushed stone G1	35 mm asphalt concrete 140 mm G1 base 255 mm cemented subbase 125 mm modified G6 subgrade	
303a2	TR86	Crushed stone G2	See Appendix A for the structural and instrumentation detail of these test sections	Data from these test sections used in this report to study the resilient and plastic deformation response of unbound aggregate.
332a2	N2/11	Crushed stone G2		
341a2	TR9/7	Crushed stone G2		
327a3	N2/23	Crushed stone G2		
398a4	Road D2388	Crushed stone G2		

Table 9 Back-calculated Effective Stiffness Moduli from Maree et al.(*8*)

HVS Test Site	Base Aggregate	Wheel Load (kN)	Bulk Stress (kN)	Load Repetitions	Degree of Saturation	Base Stiffness (MPa)
P6/1	G5	20	87	10	< 50%	60
		40	148	10	< 50%	60
		60	183	10	< 50%	70
		80	272	10	< 50%	85
		100	321	10	< 50%	110
P123/1	G5	20	131	10	< 50%	40
		40	238	10	< 50%	50
		60	364	10	< 50%	55
		80	434	10	< 50%	70
		100	519	10	< 50%	80
P157/1	G2	40	264	10	< 50%	200
		70	403	10	< 50%	300
		40	266	1.00E+06	< 50%	162
		70	366	1.00E+06	< 50%	290
		40	247	1.75E+06	< 50%	178
		70	411	1.75E+06	< 50%	225
		40	210	1.94E+06	85–100 %	195
		70	253	1.94E+06	85–100 %	235
		100	490	1.94E+06	85–100 %	263
P157/2	G1	40	370	10	< 50%	335
		70	618	10	< 50%	520
		100	879	10	< 50%	725
		40	370	4.80E+05	< 50%	250
		70	625	4.80E+05	< 50%	420
		100	848	4.80E+05	< 50%	600
		40	379	1.42E+06	< 50%	260
		70	592	1.42E+06	< 50%	380
		100	846	1.42E+06	< 50%	425
		40	371	1.70E+06	50–85%	190
		70	630	1.70E+06	50–85%	230
		100	884	1.70E+06	50–85%	275

Table 10 Back-calculated Effective Stiffness Moduli for Crushed Stone Aggregate

HVS Test	MDD Position	Deflection Wheel Load (kN)	Average Bulk Stress (kPa)	Effective Base Modulus (kPa)
303a2	4	40	342	156
	12	40	335	373
341a2	3	40	306	555
		60	450	590
	7	40	491	337
		60	707	436
327a3	5	40	335	433
		70	734	708
		100	899	718
398a4	8	40	606	545
		70	889	587
	12	40	707	498
		70	999	525
101a4	Unknown	40	264	200
		70	403	300
107a4	Unknown	40	370	335
		70	618	520
		100	879	725

the HVS tests performed on pavements with crushed stone base layers listed in Table 8. In some cases, the depth deflection data from some of the MDD stacks on these test sections could not be utilized for the back-calculation of effective stiffness moduli. These data sets were omitted from the back-calculation process.

Maree primarily investigated the influence of the stress condition on the effective stiffness of the base layer material, although the data presented by him also illustrate the effect of an increase in the degree of saturation on the effective stiffness of the material. The stress parameter that Maree used is the bulk stress based on the stress stiffening law given in Equation 1:

$$M_R = K\,\theta^n \qquad \textbf{(1)}$$

Where M_R = Resilient or effective stiffness modulus (MPa)
θ = Bulk stress $\sigma_1 + \sigma_2 + \sigma_3$ (kPa)
σ_i = Principal stresses (kPa), i = 1 to 3
K, n = Regression coefficients

Figure 6 shows the relationship between the effective stiffness modulus and the average bulk stress for the natural gravel and crushed stone aggregate at the beginning of the HVS tests from the work by Maree et al. The average bulk stress was calculated from the value of the bulk stress at the top, middle and bottom of the aggregate layer.

From Figure 6, it is apparent that the effective stiffness of the natural gravel aggregate is substantially lower than that of the crushed stone aggregate. The stiffness of both the natural gravel and crushed stone aggregate increases with increasing bulk stress. The relationship between the effective stiffness modulus and the bulk stress does not seem to be the same for the two natural gravel aggregates unlike the similar relationship for the two crushed stone aggregates.

Figure 7 shows the effect of traffic loading and degree of saturation (S) on the stiffness of the crushed stone aggregate base of Road P157/2. The legend of Figure 7 refers to the number of wheel load repetitions applied to the test section. The degree of saturation was less than 50 percent up to about 1.4 million load repetitions, after which water was applied to the test section and the degree of saturation of the aggregate base layer was reported by Maree et al. as being between 50 and 85 percent. Increases in both the traffic loading and degree of saturation caused a decrease in the effective stiffness of the aggregate base layer. This trend of decreasing stiffness with increasing traffic and moisture has manifested on most of the HVS tests on aggregate base layers in South Africa.

Figure 8 shows the effective stiffness results for crushed stone aggregate from Table 10 plotted against the average bulk stress. Although there is a general increase in the effective stiffness of the crushed stone aggregate with increasing bulk stress, a regression model of the type listed in Equation 1 yields a poor correlation between the effective stiffness and the bulk

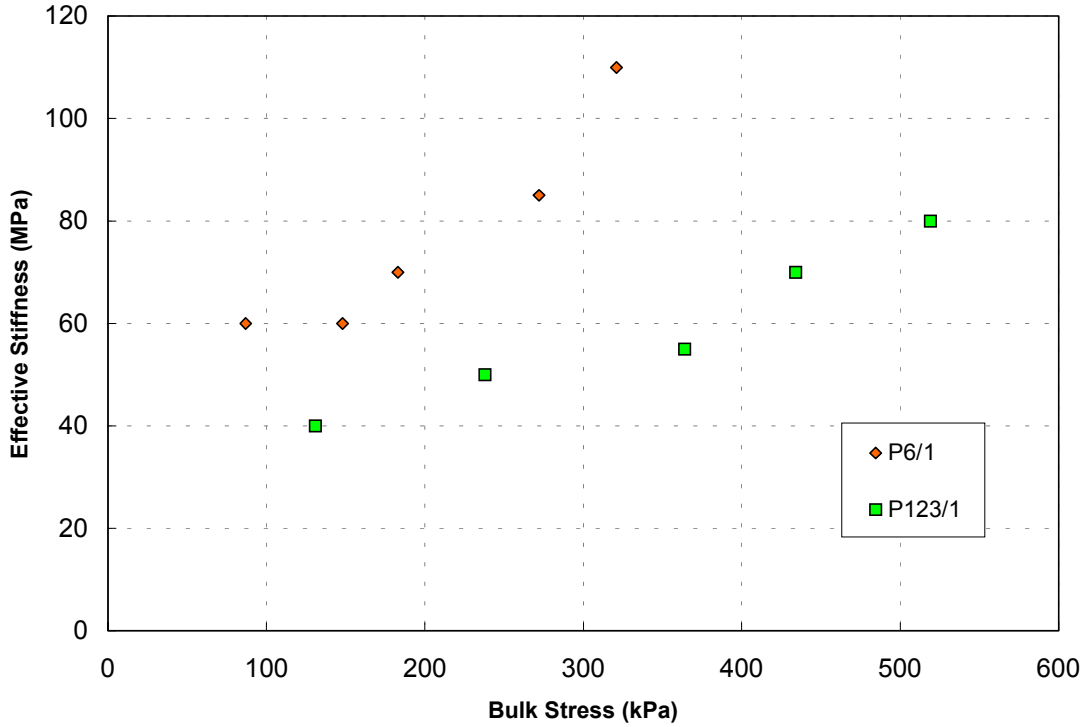

Figrue 6a. Natural gravel aggregate.

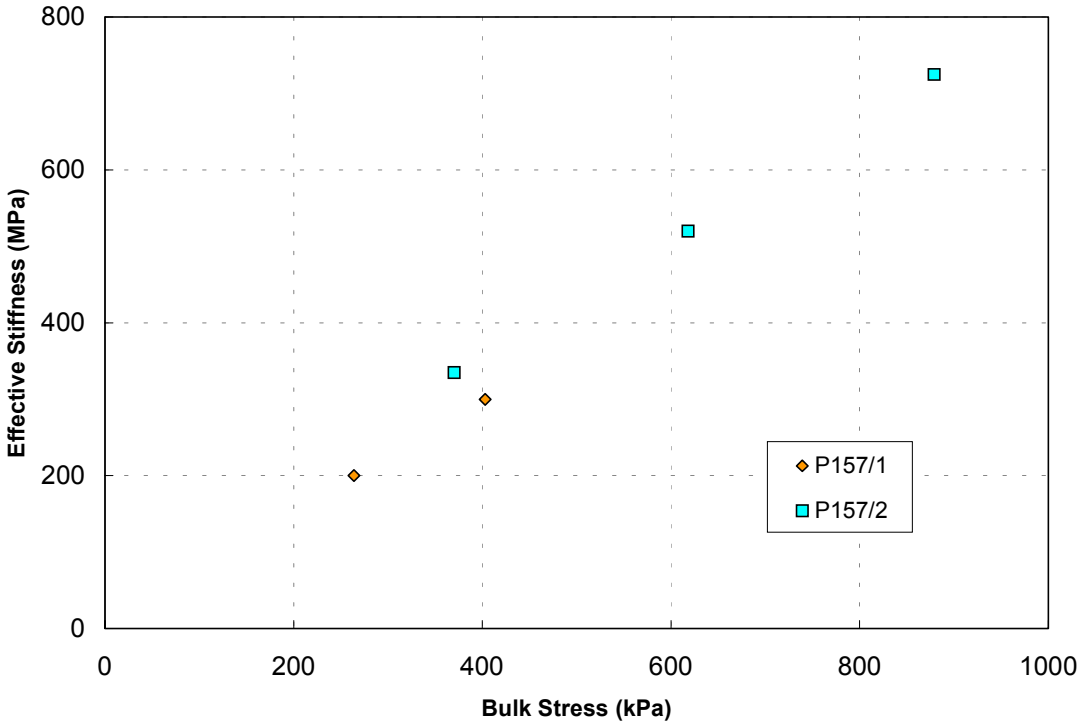

Figure 6b. Crushed stone aggregate.

Figure 6. The relationship between the bulk stress and effective stiffness modulus of natural gravel and crushed stone aggregate.

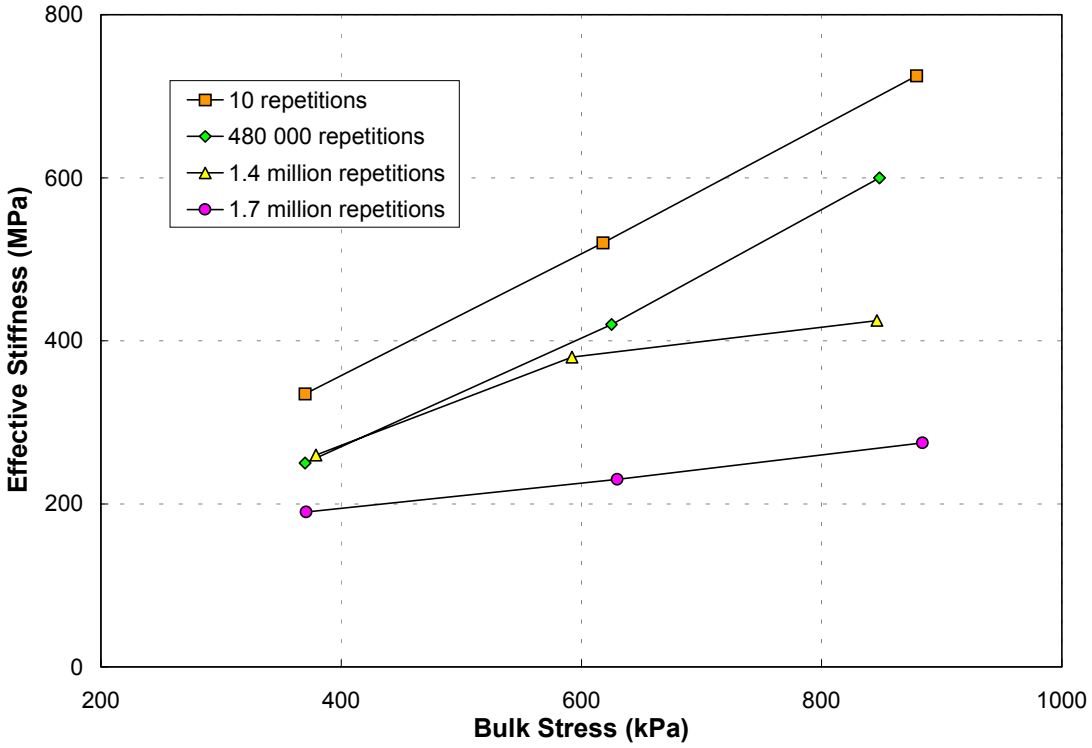

Figure 7. The effect of traffic loading and degree of saturation on the stiffness of the crushed stone aggregate from Road P157/2.

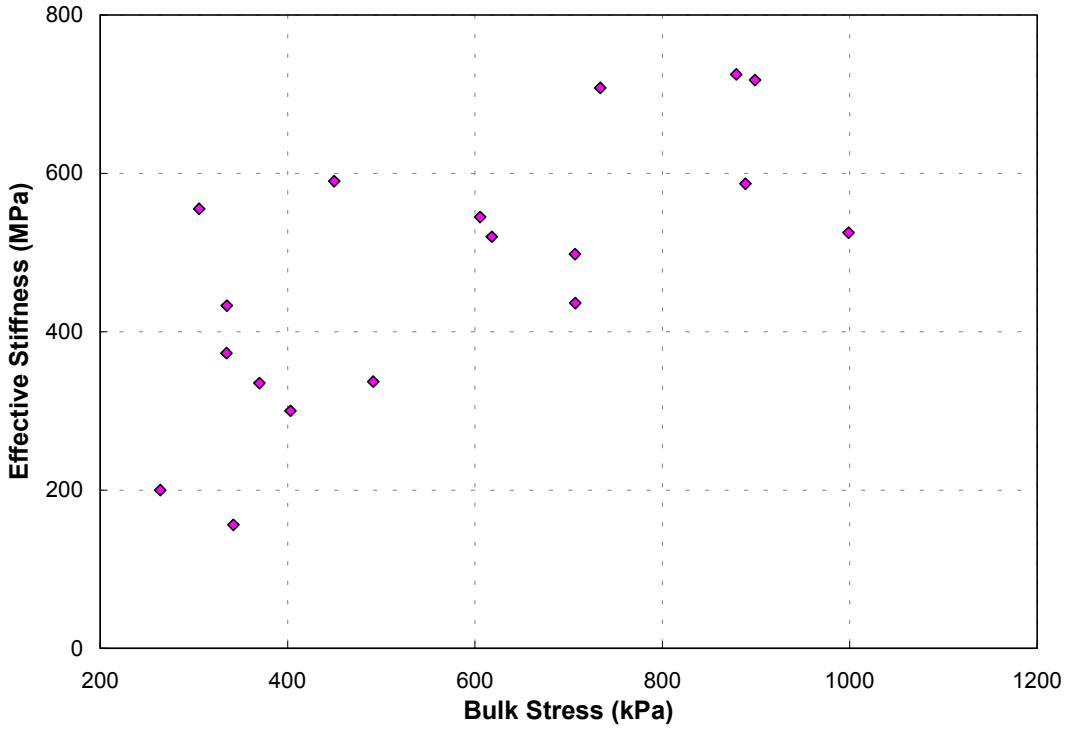

Figure 8. The relationship between the effective stiffness and bulk stress of crushed stone aggregate from a number of HVS tests.

stress. This poor correlation is caused by the fairly large amount of variation in effective stiffness at any given bulk stress value. The effect of variation in density and moisture content or degree of saturation has not been isolated from the data in Figure 8 because of the difficulty associated with determining the exact density and degree of saturation associated with each HVS test and different points on the HVS test section. Laboratory test data presented in Section 4 of this report illustrate the effect that density and degree of saturation have on the effective stiffness of crushed stone aggregate.

Figure 9 provides additional information on the effect of increased traffic loading and moisture content on the effective stiffness of a crushed stone aggregate base on HVS test section 398a4. The trafficking load sequence for test 398a4 consisted of 200,000 repetitions of a 40-kN dual wheel load followed by 200,000 repetitions of a 70-kN dual wheel load. Water was allowed to pond in 100-mm diameter holes drilled into the base layer next to one half of the HVS test section for a further 100,000 repetitions of a 70-kN dual wheel load (similar to the wetting of Goal 5 test sections in California [*3–6*]). The initial stiffness of the aggregate base layer was between 600 and 900 MPa but this soon reduced to values between 400 and 600 MPa for the duration of the 40-kN loading phase. Depth deflection data were recorded for a 40- and 70 -N dual wheel load during the 70-kN trafficking load phase. The effective stiffness of the aggregate base increased slightly under the effect of the highly overloaded 70-kN dual wheel load with the modulus at a 70-kN deflection load being higher than at a 40-kN load, again confirming the stress stiffening behavior of unbound aggregate. The effective stiffness of the aggregate base layer reduced to values below 400 MPa for both wheel loads during the wet phase of the test, highlighting the detrimental effect of moisture on the stiffness of an unbound aggregate layer.

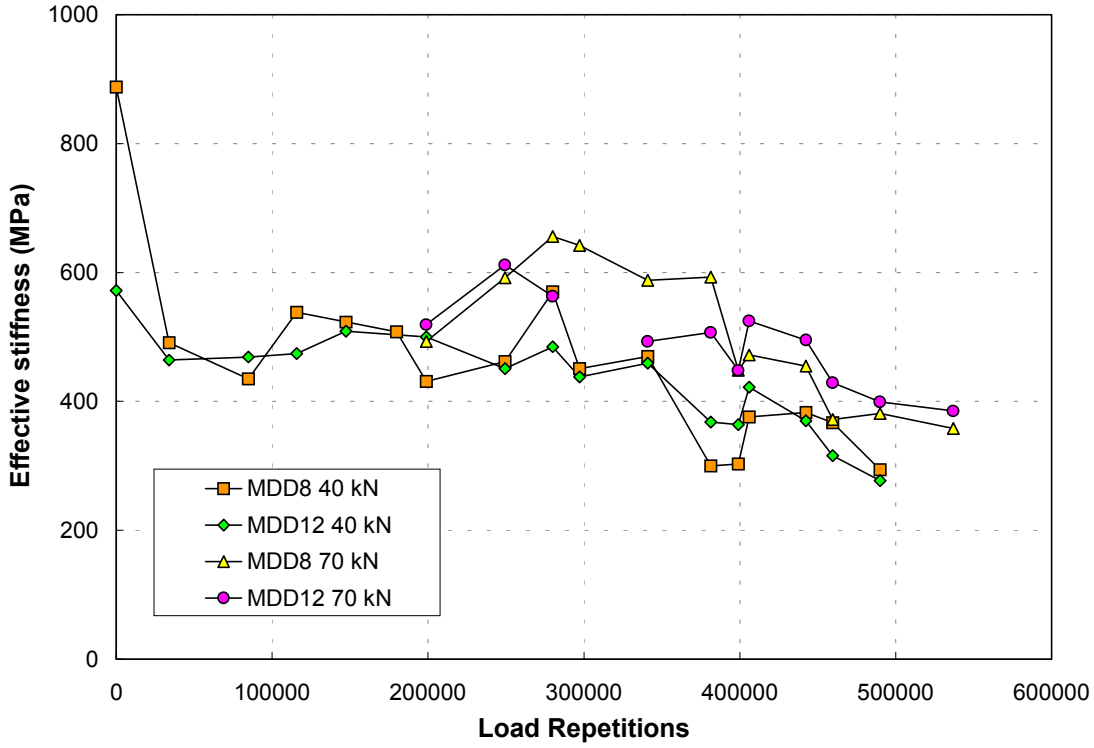

Figure 9. The effective stiffness modulus of crushed stone aggregate for the duration of HVS test 398a4.

The low permeability of the crushed stone aggregate base largely prevented water from entering the base layer.

3.2 Permanent Deformation Response of Unbound Aggregate Under HVS Testing

In addition to the depth deflection data, each MDD stack produced a set of permanent vertical MDD displacement results. This is achieved by recording the voltage output from the MDD modules at rest at various stages during the test. Various studies have been completed on the analysis of the MDD displacement and permanent deformation data generated by an HVS test.(*7, 9, 10*) In this case, the function listed in Equation 2 was fitted to the MDD displacement data of the HVS tests listed in Table 8.

$$PD = m\,N + a\left(1 - e^{-bN}\right) \quad \textbf{(2)}$$

Where PD = permanent vertical MDD displacement
N = number of load repetitions
a,b,m = regression coefficients
e = base of the natural logarithm

This function allows for two behavioral phases: an initial exponential bedding-in phase and a long-term linear rate of increase in the permanent vertical MDD displacement as is illustrated in Figure 10.

Equation 2 has an initial slope equal to the product of the two regression coefficients *a* and *b*, a curvature determined by the value of *b*, an eventual linear slope equal to the regression coefficient *m*, and an intercept with the Y-axis represented by the regression coefficient *a*. The bedding-in phase, represented by the coefficient *a* and the eventual deformation rate, represented by coefficient *m* are the two important parameters in the process of evaluating the permanent MDD displacement data for an HVS test. Once the initial bedding-in (*a*) and the eventual rate of permanent deformation (*m*) are known, it is possible to calculate the number of repetitions that would be required to induce a certain amount of plastic strain in an unbound aggregate layer bearing capacity.

Table 11 gives the bedding-in, eventual deformation rate, and the base bearing capacity for 20 mm permanent base layer deformation for the HVS tests sections listed in Table 8 at a number of MDD locations at which the permanent deformation of the aggregate base layer was recorded.

The thickness of the base layers of the HVS test sections listed in Tables 8 and 11 differed and the results from Table 11 were converted to plastic strain values by dividing the bedding-in deformation and the rate of deformation by the original thickness of the layer. Figure 11 shows the plastic deformation and base bearing capacity results obtained from this process.

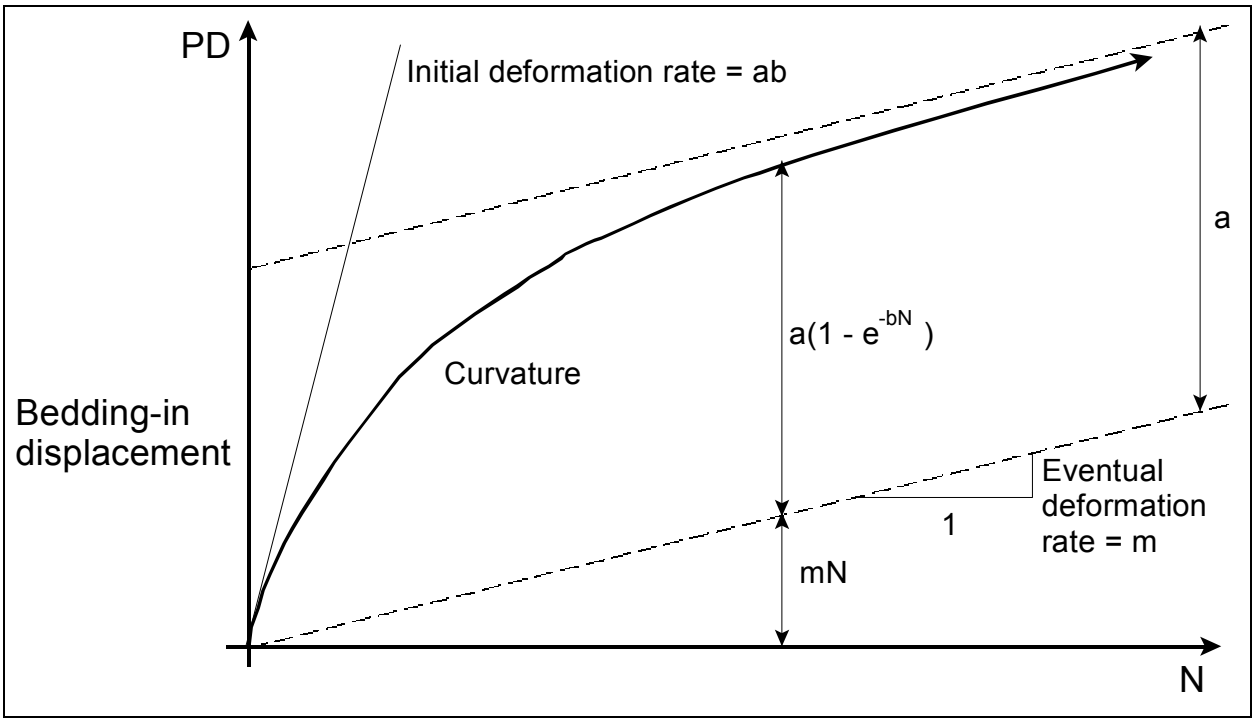

Figure 10. Illustration of typical base permanent deformation (rutting) behavior.
Note: PD = permanent deformation (rut depth or permanent vertical strain).

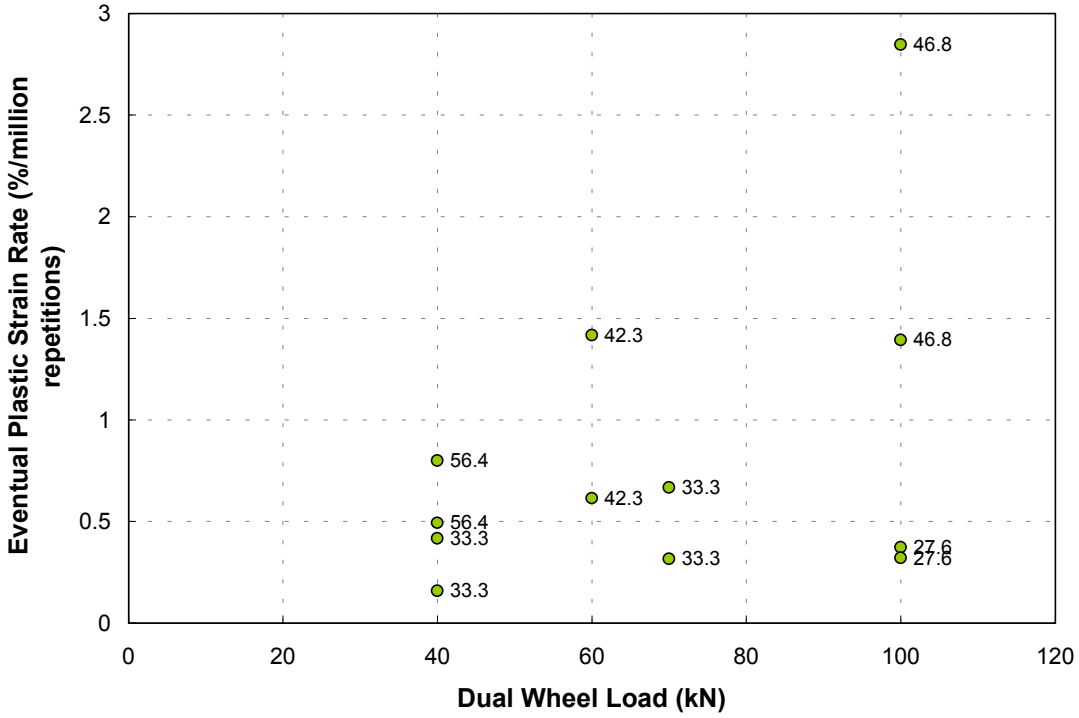

Figure 11a. Plastic strain rate.

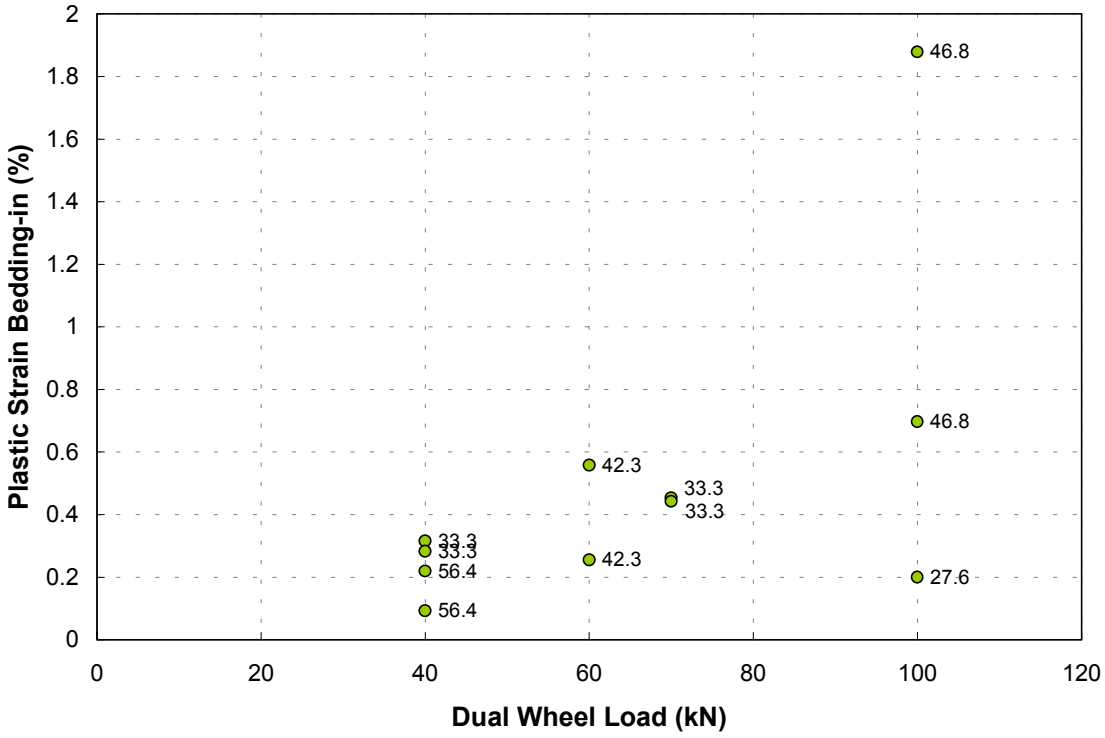

Figure 11b. Bedding-in plastic strain.

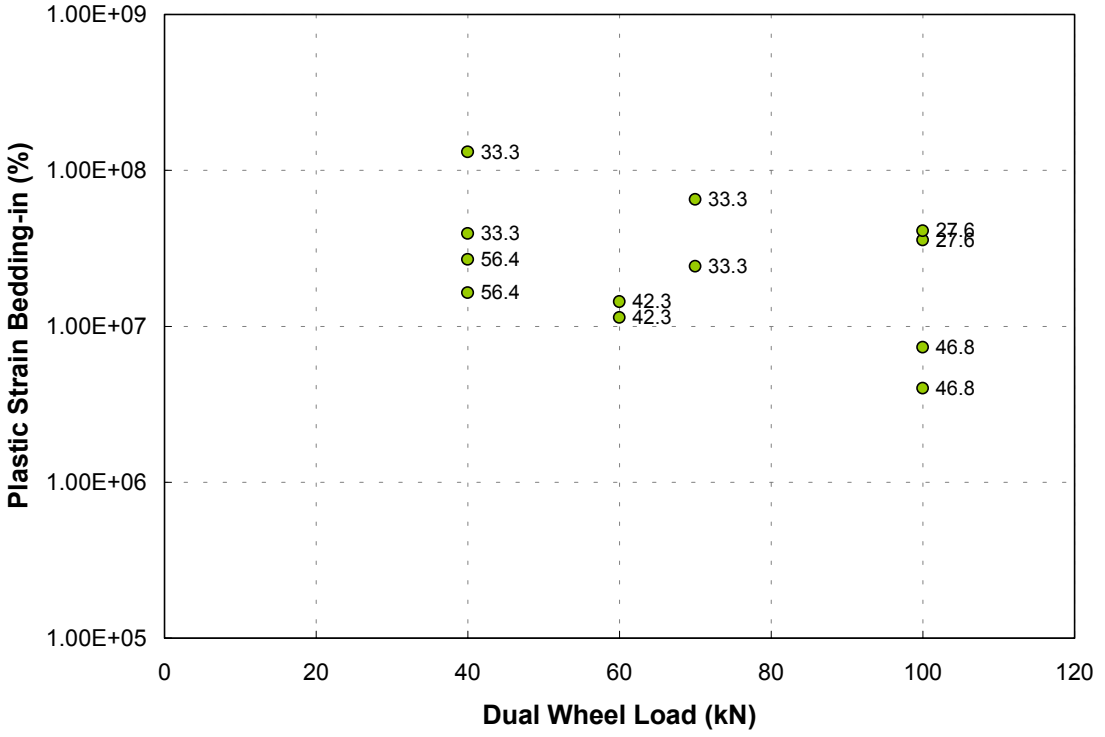

Figure 11c. Base bearing capacity for 20 mm plastic deformation of the base layer.

Figure 11. Bedding-in plastic strain, plastic strain rate, and bearing capacity results for a number of crushed stone aggregate layers determined from HVS testing.

Table 11 Base Bedding-in Displacement, Deformation Rate, and Bearing Capacity Results for a Number of Crushed Stone Aggregate Base Layers from HVS Test Sections

HVS Test No.	Wheel Load (kN)	Relative Density (% Modified AASHTO)	Moisture Content Ratio (%)	MDD Location 1	MDD Location 2	MDD Location 3
				Base Bedding-in Displacement (mm)		
303a2	100	97.8	27.6			0.30
332a2	40	99.5	56.4	0.14		0.33
341a2	60	101.0	42.3		0.67	0.56
327a3	100	97.7	46.8	3.10		1.15
398A4	40	98.8	33.3		0.30	0.34
398A4	70	98.8	33.3		0.43	0.53
				Base Eventual Deformation Rate (mm/million repetitions)		
303a2	100	97.8	27.6	0.6		0.5
332a2	40	99.5	56.4	0.7		1.2
341a2	60	101.0	42.3		1.7	1.4
327a3	100	97.7	46.8	2.3		4.7
398A4	40	98.8	33.3		0.2	0.5
398A4	70	98.8	33.3		0.3	0.8
				Base Bearing Capacity (repetitions)		
303a2	100	97.8	27.6	3.57E+07		4.10E+07
332a2	40	99.5	56.4	2.68E+07		1.64E+07
341a2	40	101.0	42.3		1.05E+07	1.00E+07
341a2	60	97.7	46.8		1.14E+07	1.44E+07
327a3	100	98.8	33.3	7.34E+06		4.01E+06
398A4	40	98.8	33.3		1.31E+08	3.93E+07
398A4	70				6.52E+07	2.43E+07

The data labels associated with each of the data points indicate the moisture content of the aggregate material expressed as a ratio of the field compaction water content over the optimum compaction moisture content of the material (modified AASHTO compaction). An increase in wheel load and moisture ratio causes an increase in the bedding-in plastic strain and the eventual plastic strain rate of the unbound aggregate material.

No clear trend could be established between the density of the material and the plastic deformation characteristics. The laboratory test results presented in Section 4 provide a better

opportunity for studying the effect of density and saturation on the permanent deformation characteristics of unbound aggregate as these parameters are better controlled under laboratory conditions.

3.3 Permeability of an Unbound Aggregate Base and Drainable Subbase on an HVS Test Section

It is evident from the data presented in Section 2 that the moisture content or degree of saturation has an influence on the effective stiffness and permanent deformation of unbound aggregate. The degree of saturation is in turn determined principally by the supply of water to the material, and secondarily by the permeability of the material, which will allow or prevent the moisture from entering the material.

Van der Merwe investigated the use of a permeable subbase drainage layer on HVS Test Section 303a2.(*11*) The detail of the pavement structure for Section 303a2 is shown in Appendix A. The subbase drainage layer was constructed from the same crushed stone aggregate used for the base layer but the gradation was not adjusted to meet the requirement for G1 and G2 aggregate. The gradation of the base and subbase aggregate, which was basically from the same source, influenced both the density to which the material could be compacted and the permeability of the material. Table 12 provides information on the gradation, density, and moisture content of the base and subbase layer aggregate for Section 303a4.

Figure 12 shows the gradation of the base and subbase aggregate compared to the gradation envelope control points for a 37.5-mm maximum size aggregate for G1 to G3 material. Table 13 lists the permeability coefficient of the base and subbase aggregate as a function of the relative density of the material. The data from Table 13 is shown in Figure 13. The effect of gradation and density on the permeability of unbound aggregate is clearly illustrated by the data

Table 12 Gradation, Density, and Moisture Content Properties of the Crushed Stone Aggregate from the Base and Drainable Subbase Layers from Section 303a2

Pavement Layer		**Base**	**Drainable Subbase**
Reference density and moisture content	Maximum mod. AASHTO density (kg/m3)	2198	2027
	Optimum moisture content (%)	7.7	9.9
	Apparent density (kg/m3)	2658	2643
Gradation	Sieve size (mm)	**Percentage passing (percent)**	
	37.5	100.0	100.0
	26.5	85.3	85.0
	19.0	69.0	70.0
	13.2	56.0	55.7
	4.75	35.0	29.7
	2.0	25.5	18.7
	0.45	16.5	10.0
	0.075	5.3	5.0
Field density and moisture content	Percent modified AASHTO maximum dry density	97.8	99.9
	Percent apparent density	80.8	76.6
	Field moisture content (percent)	4.4	2.8

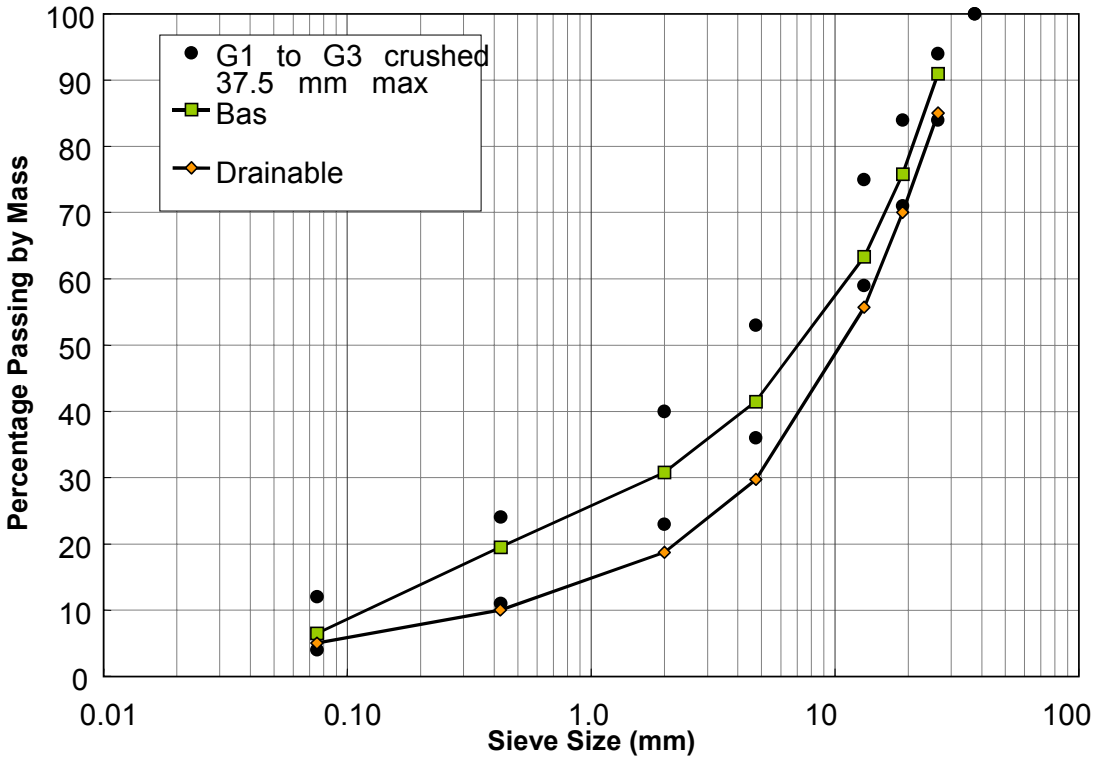

Figure 12. Gradation of the base and drainable subbase aggregate from HVS Test Section 303a2.

Table 13 **Permeability Coefficient of the Base and Subbase Aggregate from HVS Test Section 303a2 as a Function of Relative Density (Modified AASHTO Compaction)**

Relative Density (percent of Apparent Density)	Permeability coefficient (10^{-6} m/s)	
	Subbase	Base
78.0	18.200	
78.6	6.030	
79.6	3.470	
85.0		0.250
86.2		0.028
86.8		0.017
87.6		0.011
88.4		0.009

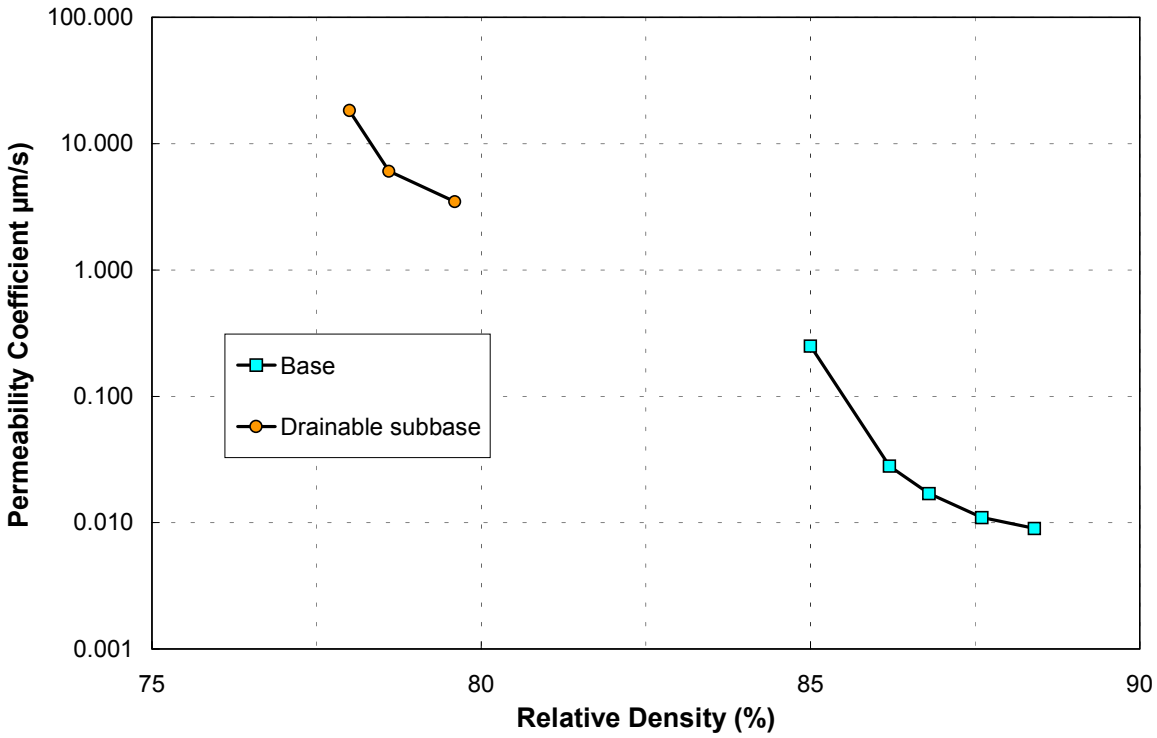

Figure 13. Permeability coefficient of the base and subbase aggregate from HVS Test Section 303a2 as a function of relative density (modified AASHTO compaction).

in Figure 13. The subbase material had a much higher permeability than the base material and the permeability of the base material reduced almost ten times with an associated increase in relative density from 85 to 86.2 percent.

Van der Merwe concluded that the structural strength of an untreated drainage layer is insufficient and the layer deformed under traffic. The permeability of the layer below the drainage layer also needs to be low enough to prevent water from entering the layer below the drainage layer. Although the permeability of the material below the drainage layer may be low enough to prevent water from entering this layer, the effective permeability of the layer may be much higher if cracks are present in the layer supporting the drainage layer.(*11*)

4.0 LABORATORY STUDIES ON UNBOUND AGGREGATE

The information in this section is largely based on three laboratory investigations of unbound aggregate. Two of these studies conducted by Maree and Theyse concentrated on the stiffness, static shear strength, and plastic deformation potential of unbound aggregate.(*12, 13*) The third study conducted by Semmelink investigated the compaction potential of unbound material including crushed stone and natural gravel aggregate.(*14*) Static and dynamic triaxial testing formed the basis of the studies by Maree and Theyse.(*12, 13*)

4.1 The Stiffness of Unbound Aggregate Under Laboratory Testing

Maree investigated the effect of several variables on the relationship between the effective stiffness or resilient modulus and the bulk stress given in Equation 2. Table 14 lists a summary of his findings.

Maree concluded that the stress condition and degree of saturation are the most important parameters determining the effective stiffness for crushed stone aggregate with density being the third most important factor. He also speculated that the degree of saturation might become the dominant factor in determining the effective stiffness of lower quality aggregate.

In addition to the stress-stiffening model from Equation 2, Maree also investigated the model shown in Equation 3, which incorporates both a stress-stiffening and stress-softening component linked to the octahedral normal and shear stress, respectively. This model is similar to the one suggested by May and Witczak (*15*) and Uzan (*16*) shown in Equation 4. Maree found a better correlation between the resilient modulus and the octahedral normal and shear stress than between the resilient modulus and bulk stress alone.

Table 14 Factors Affecting the Relationship between the Resilient Modulus and the Bulk Stress Condition of Unbound Aggregate

Factor	Change in Factor	Influence on		
		K	n	M_R
Duration of load pulse	0.1 to 1.0 s	No effect	No effect	No effect
Frequency of load pulse	0.3 to 1.0 Hz	No effect	No effect	No effect
Number of load cycles	Increase in load cycles	0–20% higher	No effect to a slight reduction	Up to a 20% increase
Load history	-	No effect	No effect	No effect
Confining pressure	Constant vs. pulsed	No unique effect detected	No unique effect detected	Constant pressure slightly overestimates MR
Sample density	increase from 82.6 to 87.5% of apparent density	100% increase	15% reduction	10% increase
Maximum particle size	19.5 and 37.5 mm	No effect	No effect	No effect
Percentage material < 0.075 mm	Increase in fines	Slight increase	Slight increase	Optimum at 9% fines
Particle shape	Increase in angularity	Not determined	Not determined	Slight increase
Surface texture	More course	Not determined	Not determined	Slight increase
Degree of saturation	increase from 20 to 90%	Up to 80% decrease	25% increase	Up to 60% decrease

$$M_R = k_1 (\sigma_{oct})^{k_2} (\tau_{oct})^{k_3} \quad \textbf{(3)}$$

Where M_R = Resilient or effective stiffness modulus (MPa)
θ = Bulk stress $\sigma_1 + \sigma_2 + \sigma_3$ (kPa)
σ_{oct} = Octahedral normal stress = $\theta/3$ (kPa)
τ_{oct} = Octahedral shear stress = 0.47 σ_d for the triaxial test (kPa)
k_i = Regression coefficients, i = 1 to 3

$$M_R = k_1 \left(\frac{\theta}{p_a} \right)^{k_2} \left(\frac{\sigma_d}{p_a} \right)^{k_3} \quad \textbf{(4)}$$

Where M_R = Resilient or effective stiffness modulus (MPa)
θ = Bulk stress $\sigma_1 + \sigma_2 + \sigma_3$ (kPa)
σ_d = Deviator stress $\sigma_1 - \sigma_3$ (kPa)
p_a = Reference stress (kPa)
k_i = Regression coefficients, i = 1 to 3

Theyse tested a crushed stone aggregate in the repeated load triaxial test as part of a laboratory project done in association with the HVS testing of several construction labor-intensive base layers. Table 15 contains the secant modulus values representing the effective stiffness or resilient modulus for a crushed stone aggregate obtained from dynamic triaxial tests for different combinations of dry density and degree of saturation.

Table 15 Resilient Modulus Values for a Crushed Stone Aggregate at Different Combinations of Density and Saturation

Dry Density (% of apparent density)	Degree of Saturation (%)	Confining Stress (kPa)	Stress Ratio (% of maximum shear strength)	Resilient Modulus or Effective Stiffness (MPa)
84.50	100.00	80	73	357
84.50	100.00	80	92	360
84.50	100.00	80	51	377
80.70	78.00	140	90	380
84.50	100.00	140	74	390
80.70	78.00	80	93	392
80.70	78.00	140	52	447
84.50	100.00	140	91	447
84.50	100.00	140	53	461
80.70	78.00	80	73	468
80.70	33.40	80	94	476
80.70	33.40	140	73	502
80.70	78.00	140	74	512
80.70	33.40	140	52	564
80.70	33.40	140	93	569
84.50	43.50	140	72	620
84.50	43.50	140	52	651

Theyse investigated the effect of dry density and degree of saturation on the effective stiffness of the crushed stone material in addition to the effect of the stress condition on the effective stiffness. The stress condition is represented by the confining pressure, which will tend to cause stress-stiffening behavior, and the stress ratio, which will cause a reduction in effective stiffness as the maximum shear strength of the material is approached. The function in Equation

5 was fitted to the data from Table 15. Figure 14 shows a plot of the observed and predicted values for the resilient modulus of the crushed stone aggregate that was tested.

$$M_R = -527.96 + 14.04\ RD - 2.72\ S + 0.82\ \sigma_3 - 0.87\ SR \quad \textbf{(5)}$$

R^2 = 81.2 % and Standard Error of Estimate (SEE) = 45.4 MPa

Where M_R = Resilient modulus (MPa)
RD = Relative density (% of apparent density)
S = Degree of saturation (%)
σ_3 = Confining pressure or minor principal stress (kPa)
SR = Stress ratio (applied shear stress expressed as a percentage of the shear strength of the material at the specific confining pressure)

The four variables — relative density, degree of saturation, confining stress and stress ratio — explain about 81 percent of the variation in the effective stiffness of the crushed stone aggregate. According to the regression model, an increase in the relative density and confining pressure will result in an increase in the effective stiffness of the material. In addition, an

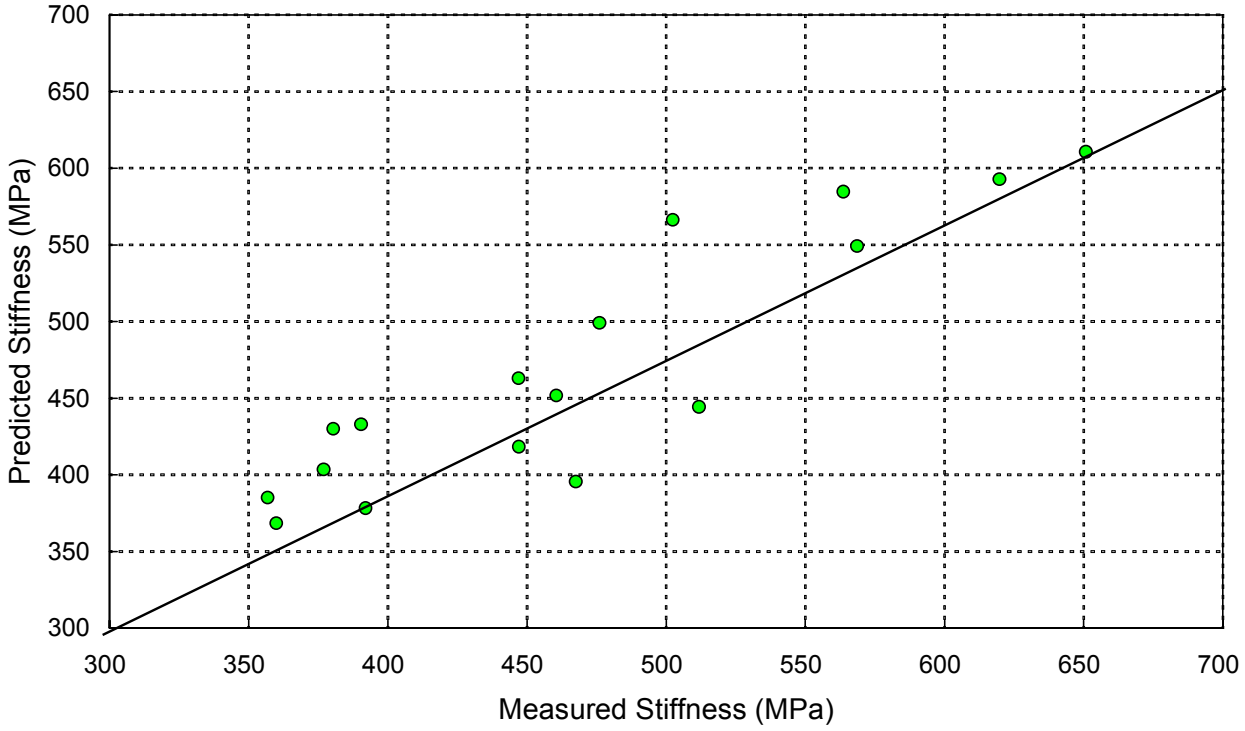

Figure 14. The observed and predicted values of the resilient modulus for a crushed stone aggregate.

increase in the degree of saturation and stress ratio will result in a decrease in the effective stiffness of the material. The rate of change in effective stiffness associated with a unit increase in relative density is the highest, followed by the rate of decrease associated with the degree of saturation. The rates of change associated with a unit change in confining pressure and stress ratio are of the same order of magnitude. The relative density therefore appears to be the variable that will most influence the effective stiffness. The range of practical values for the relative density (80–88 percent or apparent density) is, however, much narrower than that of the degree of saturation (30–100 percent) and the degree of saturation may therefore have the biggest impact on the effective stiffness of the crushed stone material.

The range of laboratory stiffness values reported in Table 15 agrees well with the range of HVS back-calculated effective stiffness values reported in Table 10 and shown in Figure 8, except for two relatively low values from HVS Tests 101a4 and 303a2.

In summary, it appears that the range of effective stiffness values for crushed stone aggregate may be expected to vary from about 350 to 700 MPa based on HVS and laboratory results. A major portion of this variation in effective stiffness may be explained by variation in the relative density and the degree of saturation of the material and stress condition imposed on the material. Most of the more recent resilient modulus models for unbound aggregate allow for a combination of stress-stiffening and stress-softening behavior for unbound aggregate. The stress-stiffening behavior is normally associated with an increase in the confinement of the material that may be quantified by the minor principle stress, the bulk stress, or the octahedral normal stress. The stress-softening behavior is normally associated with the level of shear stress imposed on the material and may be quantified by the deviator stress, octahedral shear stress, or

the stress ratio expressing the applied shear stress as a percentage of the shear strength of the material for the given value of the minor principle stress.

4.2 Static Shear Strength Parameters of Unbound Aggregate

Maree (*17*) re-analyzed existing static triaxial data and performed additional static triaxial tests on several crushed stone and natural gravel aggregates from which the influence of several parameters on the static shear strength parameters of unbound aggregate were identified. Table 16 gives a summary of these parameters and their influence on the shear strength parameters.

Table 16 Factors Affecting the Relationship Between the Resilient Modulus and the Bulk Stress Condition of Unbound Aggregate

Factor	Change in Factor	Influence on:		
		Shear Strength	Cohesion	Internal Friction Angle
Density	Increase	Significant increase	Significant increase	Considerable increase
Degree of saturation	Reduction	Significant increase	Significant increase	No effect
Shape of gradation curve	Change in Talbot n-value from 0.5 to 0.3	Increase	Considerable increase	Reduction
Maximum particle size	9.5 to 37.5 mm	Increase	Increase	Increase
Percentage fines	1 to 9 %	Increase	Considerable increase	Increase
	9 to 15 %	Reduction	Reduction	Reduction
Plasticity of fines	Non-plastic to plastic	Reduction	Reduction	Reduction
Type of aggregate	Crushed stone to natural gravel	Reduction	Significant reduction	Significant reduction
Durability of aggregate	High to low durability	Reduction	Reduction	Reduction
Particle shape	From round to angular	Increase	No effect	Increase
Surface texture	Smooth to rough	Increase	Uncertain	Increase
Type of fines	Crusher dust replaced by sand	Reduction	Significant reduction	No effect

Maree again concluded that density and moisture (or degree of saturation) are the two most important parameters affecting the shear strength and shear strength parameters of unbound aggregate.

Theyse (*13*) did extensive triaxial testing on a crushed stone aggregate to determine the effect of relative density and degree of saturation on the shear strength parameters of the material. Tables 17 and 18 show the cohesion and friction angle results as a function of the moisture content and relative density in terms of percentage of apparent density. The moisture content levels reported in Tables 17 and 18 were converted to degree of saturation values in order to produce the relationships between the shear strength parameters, relative density, and degree of saturation given in Equations 6 and 7 and illustrated in 15 and 16. These results, which are valid for one specific crushed stone aggregate, indicate that the relative density and degree of saturation affect both the friction angle and cohesion of the crushed stone aggregate.

Table 17 Cohesion (kPa) results for crushed stone aggregate

Relative Density (%)	**Cohesion (kPa)**		
	Moisture Content (%)		
	3	**5**	**7**
81	94.9	68.1	28.1
83	120.5	35.6	25.7
85	102.8	51.1	43.0

Table 18 Friction Angle Results for the Crushed Stone

Relative Density (%)	**Friction Angle (degrees)**		
	Moisture Content (%)		
	3	**5**	**7**
81	53.1	48.6	49.4
83	51.4	50.7	50.1
85	54.6	51.4	47.7

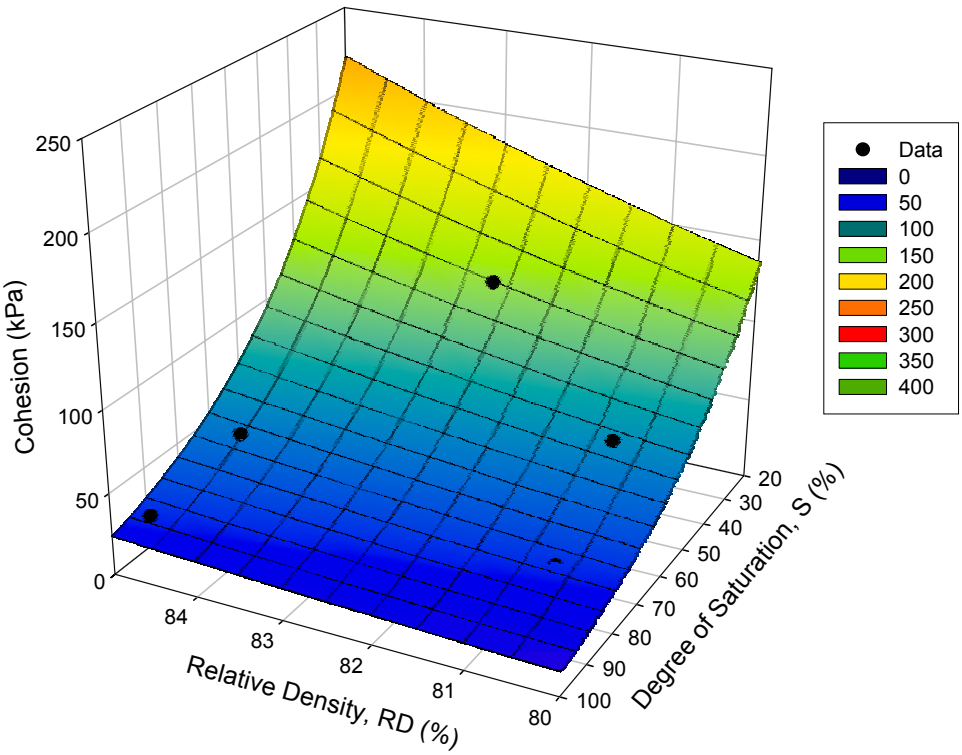

Figure 15. The relationship between the cohesion, relative density, and degree of saturation for a crushed stone aggregate.

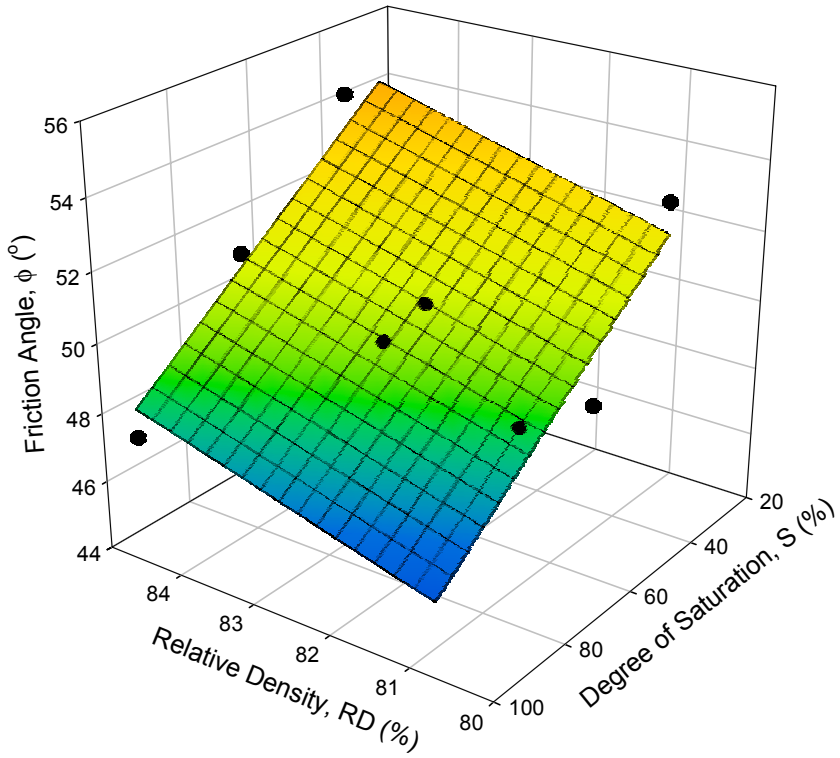

Figure 16. The relationship between the friction angle, relative density, and degree of saturation for a crushed stone aggregate.

$$C = 0.0107\, e^{12.12\, RD}\; e^{-2.30\, S} \quad \textbf{(6)}$$

$R^2 = 79.9$ %; SEE = 1.346

$$\phi = 9.39 + 55.98\, RD - 7.93\, S \quad \textbf{(7)}$$

$R^2 = 70.4$ %; SEE = 1.357

where:

C	=	cohesion (kPa)
RD	=	relative density (% of apparent density)
S	=	saturation (%)
ϕ	=	friction angle (degrees)

Table 19 contains the combined static triaxial test data from the work by Maree and Theyse for both crushed stone and natural gravel aggregate. Figure 17 shows the friction angle and cohesion results plotted against relative density and degree of saturation for the combined data.

The friction angle data plotted against the relative density shows two distinct groupings of the data (Figure 17a). The relative density of the natural gravels was mostly confined to a narrow band of values between 73 and 75 percent of apparent density. The friction angle results for the natural gravels do, however, vary by a substantial amount within this narrow relative density band and there seems to be no correlation between the relative density and friction angle results. In the case of the crushed stone aggregate, although there also seems to be a poor correlation between friction angle and relative density, there is a general increase in the friction angle with increasing relative density. There does not seem to be any correlation between the degree of saturation and the friction angle for both the crushed stone and natural gravel aggregates (Figure 17b).

Table 19 Shear Strength Parameters of a Selection of Crushed Stone and Natural Gravel Aggregate

Material Classification	Relative Density, (%)	Degree of Saturation, (%)	Friction Angle, (°)	Cohesion, (kPa)
G2	80.7	55.7	48.6	68.1
G2	80.7	78.0	49.4	28.1
G2	82.6	37.9	51.4	120.5
G2	82.5	63.2	50.7	35.6
G2	82.6	72.6	50.1	25.7
G2	84.5	72.6	51.4	51.1
G2	84.5	43.5	54.6	102.8
G2	80.7	33.4	53.1	94.9
G2	84.5	100.0	47.7	43.0
G1	87.5	90.0	57.8	43.0
G1	86.9	55.0	55.1	53.0
G1	87.0	38.0	55.2	76.0
G1	82.6	92.0	50.5	10.0
G1	86.2	80.0	57.1	16.0
G1	84.7	47.0	56.7	58.0
G2	85.3	41.0	56.1	44.0
G2	86.2	37.0	52.7	70.0
G2	86.1	42.0	53.1	48.0
G2	85.1	82.0	49.8	21.0
G2	85.6	36.0	52.1	45.0
G1	87.0	31.0	56.0	96.0
G1	87.0	90.0	53.0	16.0
G1	87.0	40.0	55.8	63.0
G1	84.0	30.0	54.2	30.5
G1	84.0	90.0	53.2	7.3
G4	73.8	24.6	51.0	74.2
G4	73.8	41.0	48.2	51.2
G10	73.5	26.2	45.6	72.4
G10	73.5	41.2	38.4	28.6
G4	74.7	47.0	52.3	35.0
G4/G5	73.5	70.0	49.8	18.0
G5	74.5	73.0	41.0	4.0
G5	72.7	46.0	43.6	18.0
G5	73.1	51.0	38.0	36.0
G5	73.5	77.0	43.0	43.0

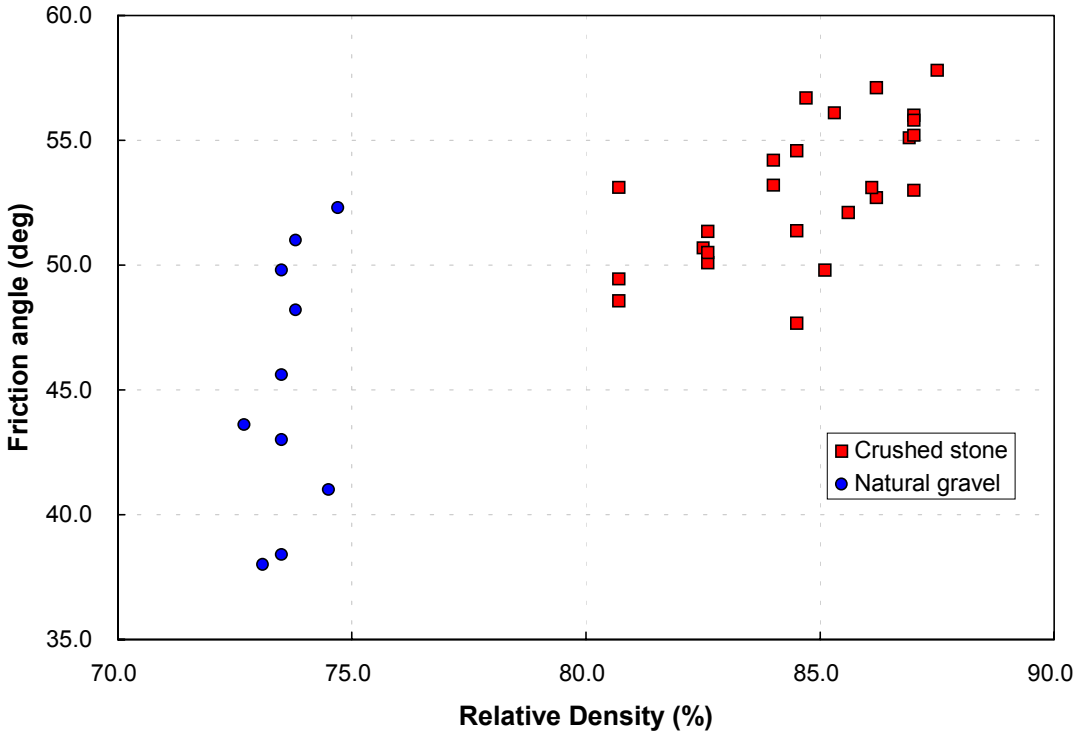

Figure 17a. Friction angle versus relative density for crushed stone and natural gravel aggregate; component effect: compaction.

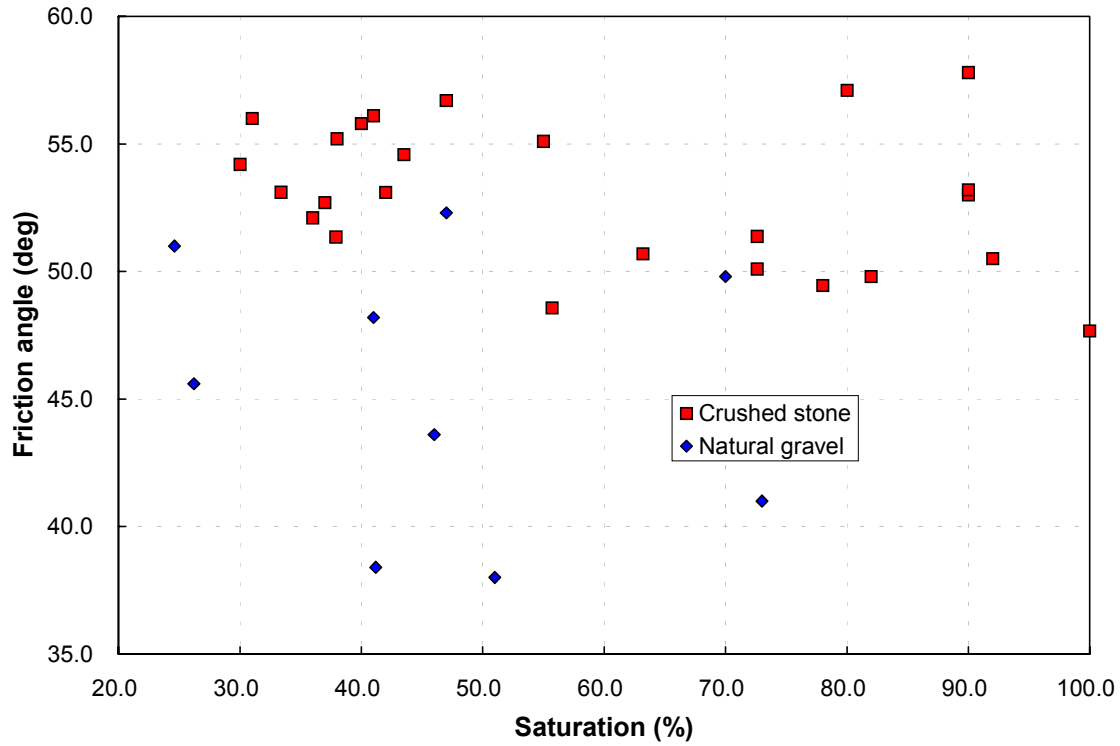

Figure 17b. Friction angle versus saturation for crushed stone and natural gravel aggregate; component effect: saturation.

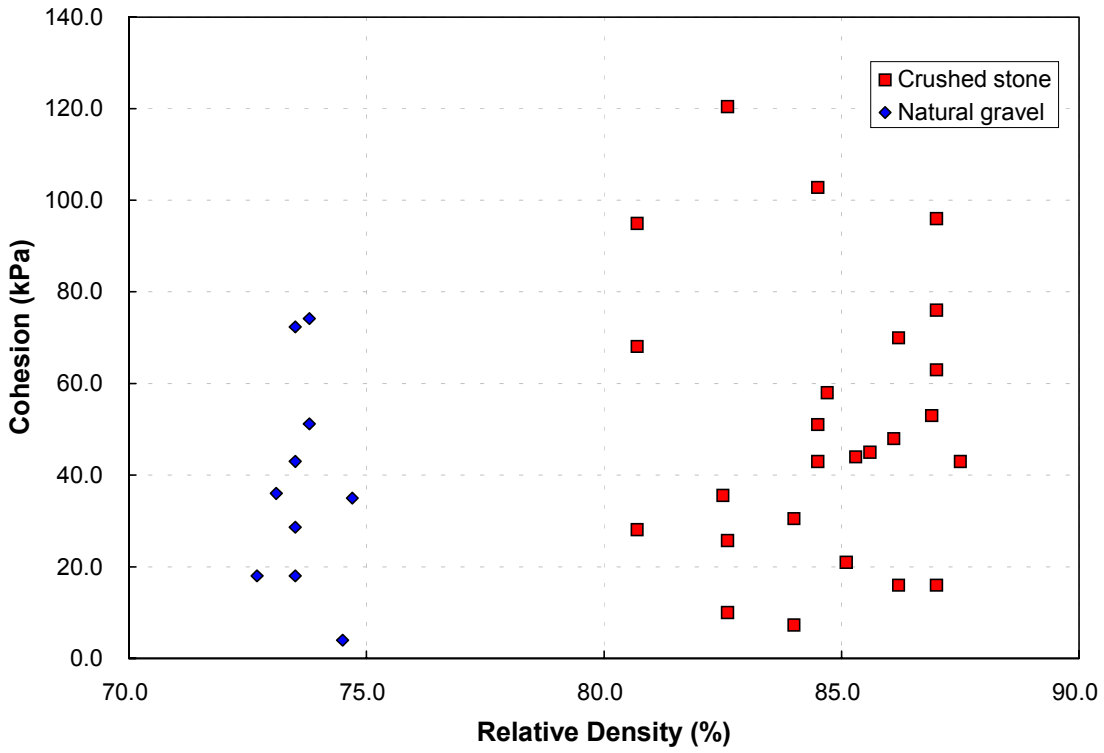

Figure 17c. Cohesion versus relative density for crushed stone and natural gravel aggregate; component effect: compaction.

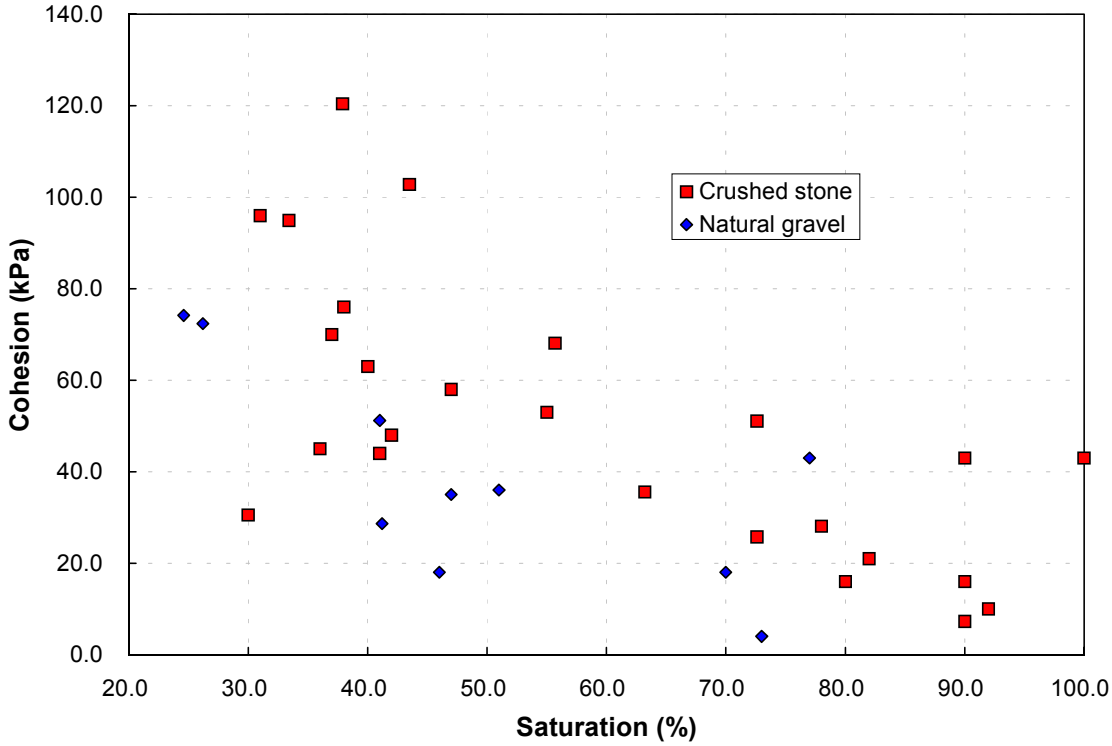

Figure 17d. Cohesion versus saturation for crushed stone and natural gravel aggregate; component effect: saturation.

Although the correlation between the degree of saturation and the cohesion of the combined data seems to be poor, there is a general trend of decreasing cohesion associated with an increasing degree of saturation (see Figure 17d). This is expected, as the cohesion should increase with decreasing degree of saturation because of apparent cohesion caused by negative pore water pressure or matric suction at the lower saturation values. There seems to be no clear trend in the combined cohesion data plotted against the relative density (see Figure 17c).

Figure 18 shows similar plots to those in Figure 17, but for the friction angle and cohesion data of the crushed stone aggregate alone. Again, although the correlation does not seem to be very good, there seems to be a general increase in friction angle with increasing relative density and a general reduction in cohesion with increasing degree of saturation. The friction angle seems to be independent of the degree of saturation and the cohesion seems to be independent of the relative density. These same trends hold for the friction angle and cohesion data of the natural gravel aggregate plotted in Figure 19.

4.3 Permanent Deformation of Unbound Aggregate

Maree (*17*) and Theyse (*13*) performed repeated load or dynamic triaxial tests on unbound aggregate in addition to the static triaxial tests to study the permanent deformation or plastic strain behaviour of these materials. The terms *permanent deformation* and *plastic strain* are used without distinction in this document. In general, permanent deformation refers to the absolute change in the linear dimensions of the sample in units of linear displacement and the plastic strain refers to the change in the linear dimensions expressed as a percentage of the original dimensions.

Both researchers found that the permanent deformation response of the triaxial samples were either stable, as shown in Figure 20a, or unstable, as shown in Figure 20b. Generally, for

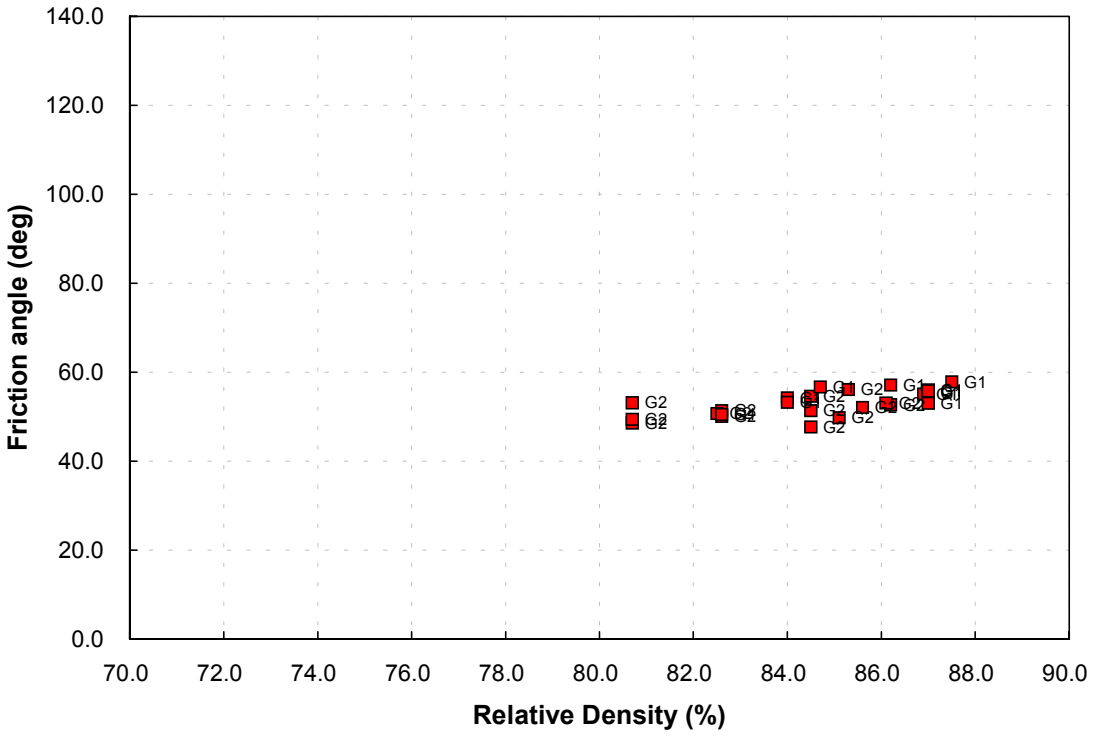

Figure 18a. Friction angle versus relative density for crushed stone aggregate; component effect: compaction.

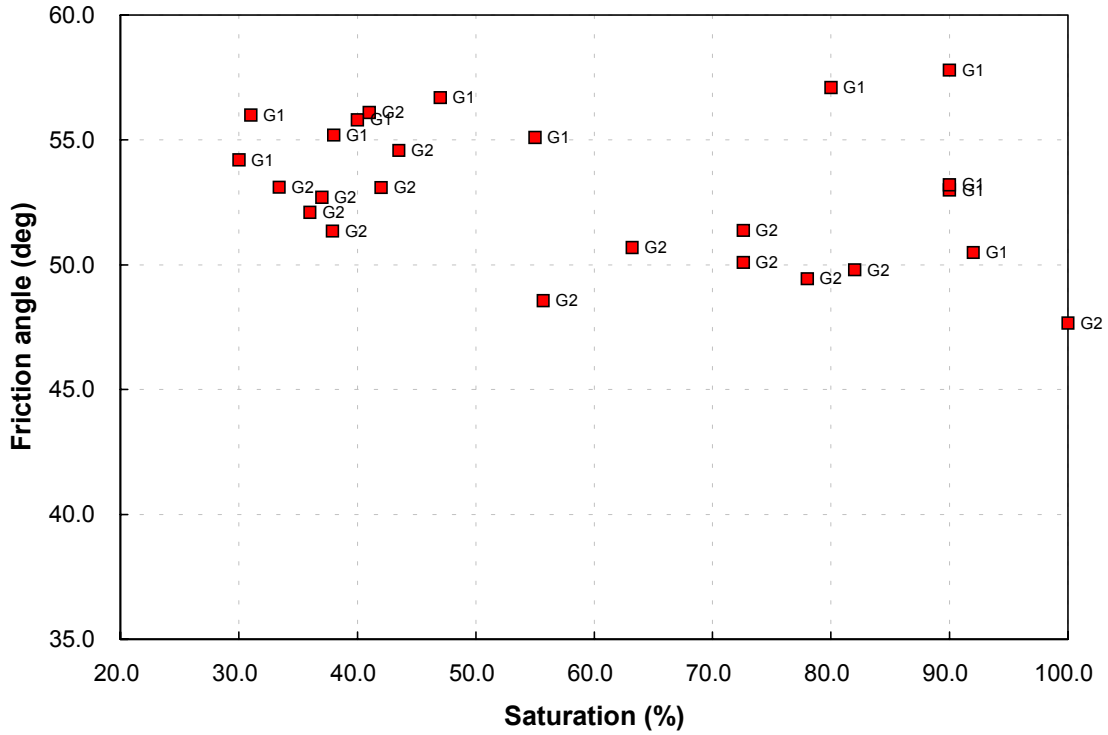

Figure 18b. Friction angle versus saturation for crushed stone aggregate; component effect: saturation.

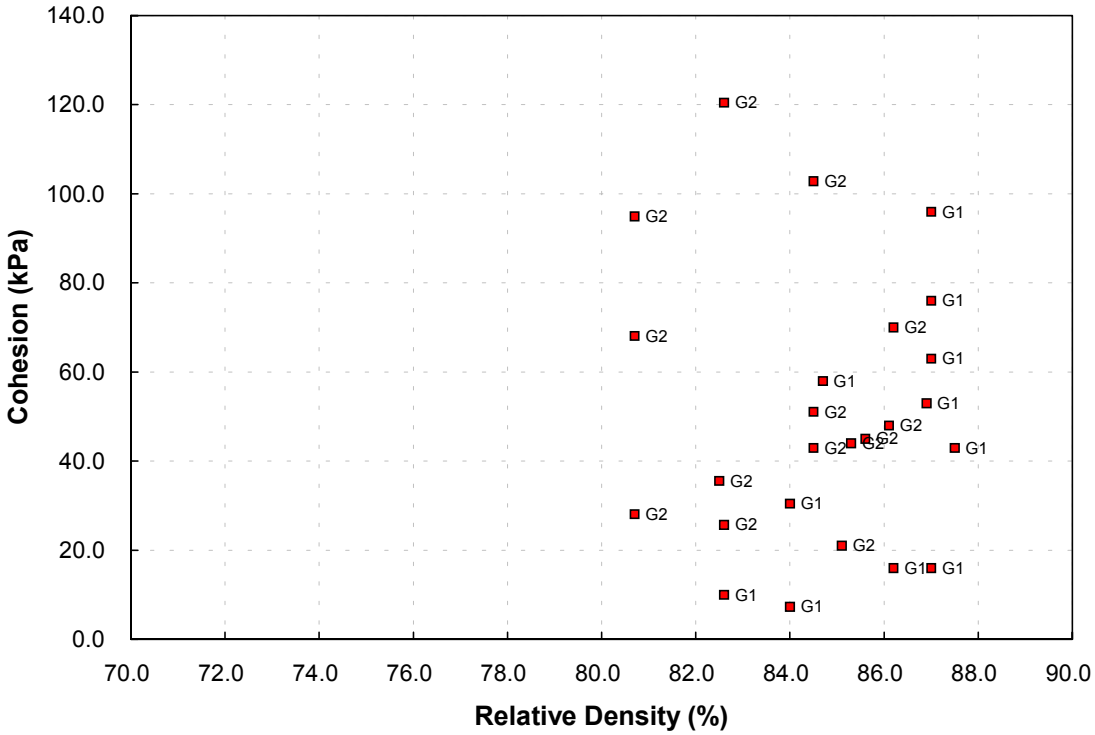

Figure 18c. Cohesion versus relative density for crushed stone aggregate; component effect: compaction.

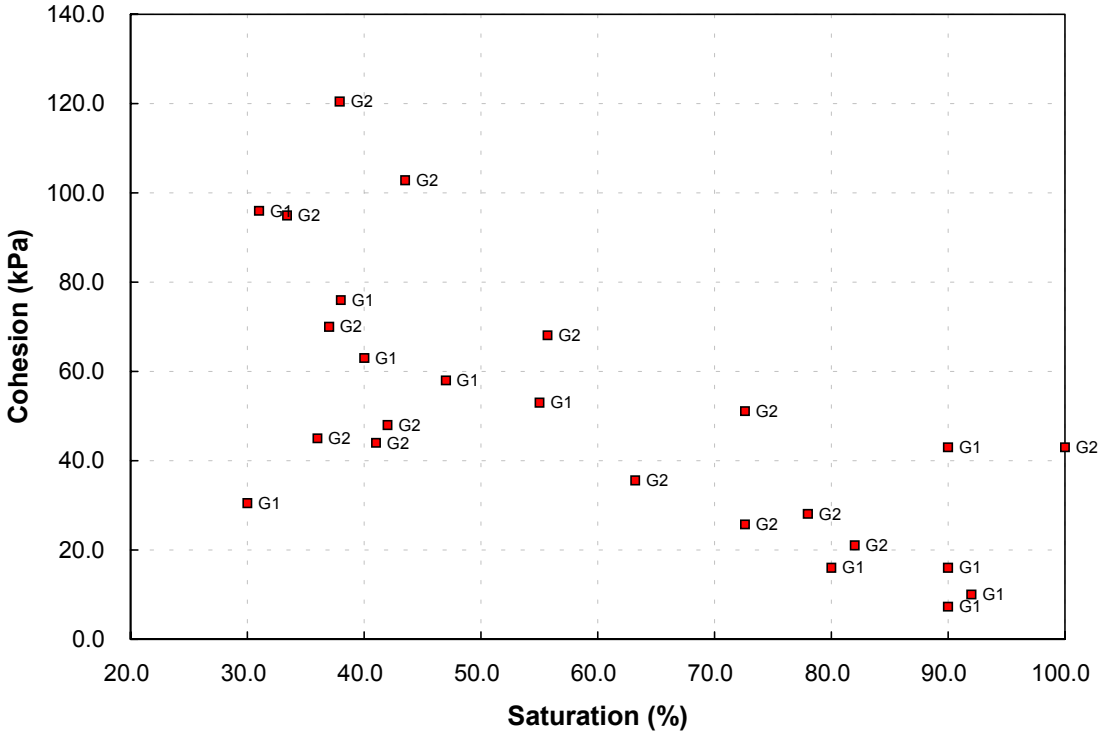

Figure 18d. Cohesion versus saturation for crushed stone aggregate; component effect: saturation.

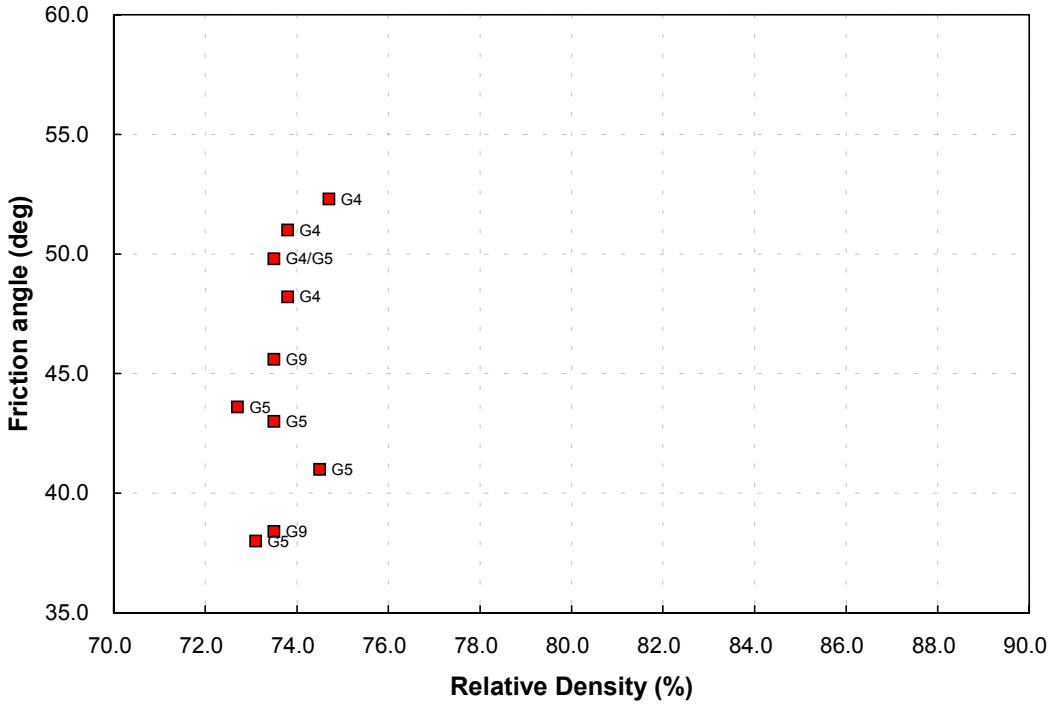

Figure 19a. Friction angle and cohesion results plotted against relative density and degree of saturation for natural gravel aggregate; component effect: compaction

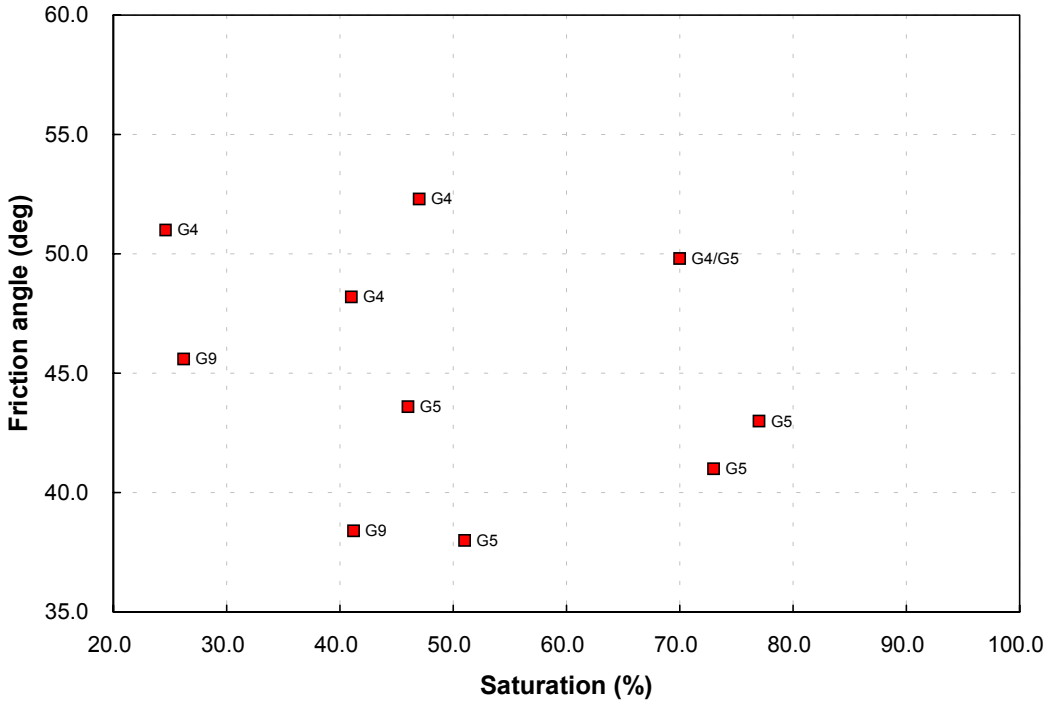

Figure 19b. Friction angle and cohesion results plotted against relative density and degree of saturation for natural gravel aggregate; component effect: saturation.

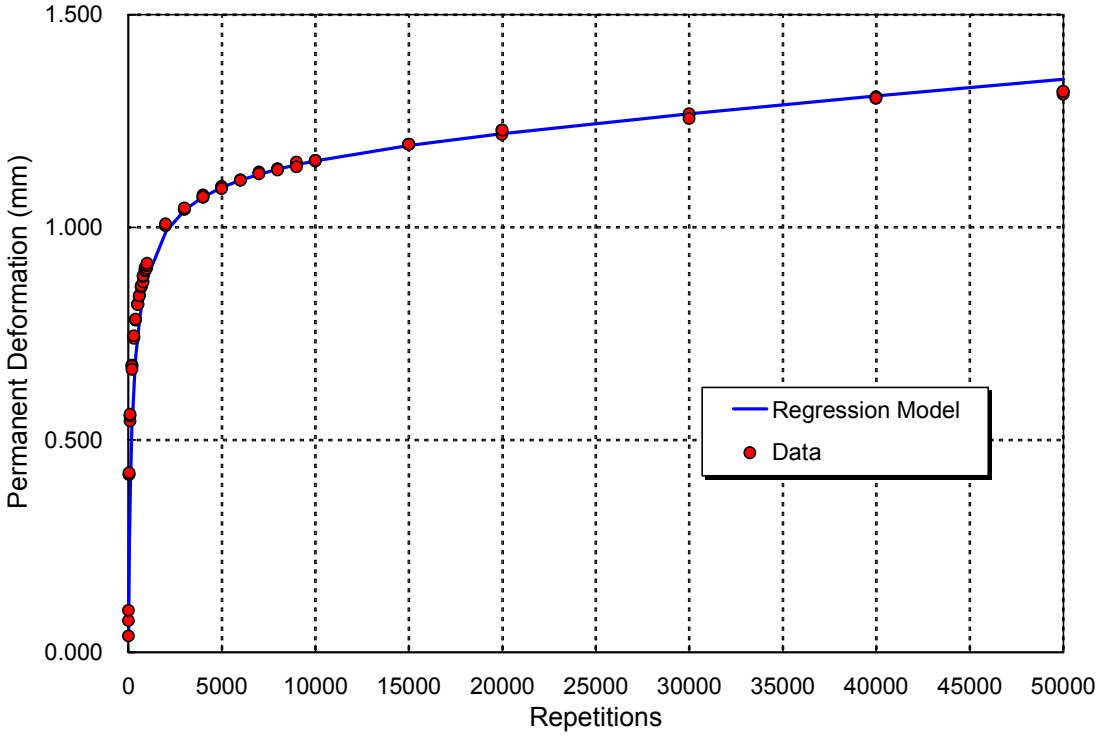

Figure 20a. Stable permanent deformation response.

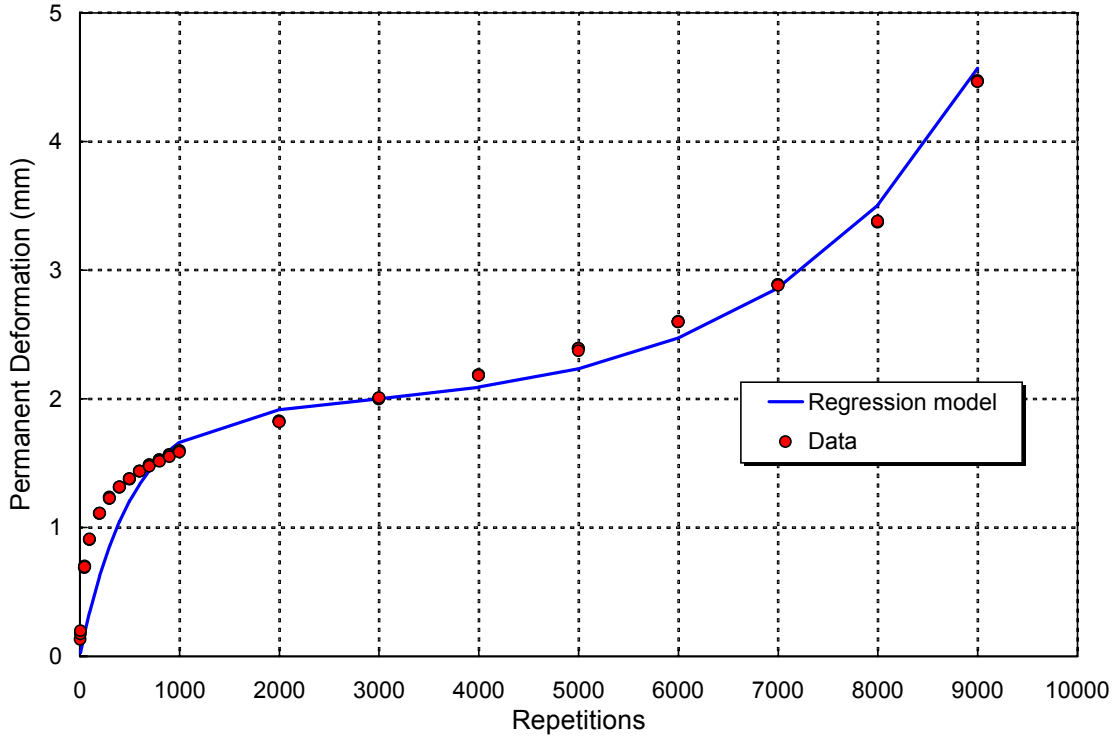

Figure 20b. Unstable permanent deformation response.

Figure 20. Stable and unstable permanent deformation response of dynamic traxial test samples.

the stable case, the permanent deformation enters a phase of a linear rate of increase after about 10,000 load cycles and thereafter remains stable. The unstable condition associated with an exponential increase in permanent deformation is normally entered within the first 10,000 load repetitions. The unstable condition never occurred after 10,000 load repetitions for any of the tests performed by Maree and Theyse.

Maree investigated the factors that determined whether a sample became unstable or remained stable. Theyse attempted to model the magnitude of the plastic strain that would occur in each of these cases using regression models. The factors having an influence on the permanent deformation of unbound aggregate that were investigated by Maree and Theyse included:

- the shear stress condition imposed on the material,
- the relative density of the material and
- the degree of saturation of the material.

4.3.1 Factors Affecting the Stability of Unbound Aggregate Under Repeated Loading

Maree used the ratio of the applied deviator stress to the maximum shear strength at a given confining pressure as a measure of the imposed shear stress condition during a repeated load triaxial test. Table 20 (*17*) gives a summary of the dynamic triaxial test results obtained by Maree.

As far as the imposed shear stress condition is concerned, the data from Table 20 indicates that the stable permanent deformation condition is maintained at stress ratio values between 58 and 93 percent of the static shear strength of the material. Maree concluded that the

Table 20 Dynamic Triaxial Test Results from Maree (*17*)

Material Type	Relative Density, (% of apparent density)	Degree of Saturation, (%)	Confining Pressure, (kPa)	Static Shear Strength, (kPa)	Maximum Values for Stable Condition	
					Repeated Deviator Stress, (kPa)	Stress Ratio, (%)
Norite	86.1	71	50	1300	750	58
	87.1	91	50	1070	600	56
	86.5	53	50	1450	1050	72
	84.0	94	50	700	420	60
	82.6	92	50	550	330	60
Quartzitic sandstone	88.0	74	100	1454	1000	69
Granite	84.9	48	100	1667	1000	60
Hornfels	85.1	39	100	1470	1000	68
Sandstone	84.8	47	100	1299	1000	77
Quartzite	85.8	43	100	1380	1280	93

relative density did not seem to have any additional effect on the permanent deformation of unbound aggregate except for a reduction in the shear strength (angle of friction) with decreasing density. On the other hand, the degree of saturation had the dual effect of reducing the shear strength (cohesion) of the material and lowering the level of the stress ratio at which the unstable condition occurred, as shown in Figure 21.

4.3.2 Empirical Modeling of the Plastic Deformation of Unbound Aggregate

Equations 8–10 provide the regression models that were fitted to the dynamic triaxial permanent deformation data by Theyse (*13*). These equations relate the permanent deformation for each individual sample to the number of load cycles that has been applied to the sample. Equations 8 and 9 may be used for the stable permanent deformation condition while Equation 10 allows for an exponential increase in the permanent deformation associated with the unstable condition.

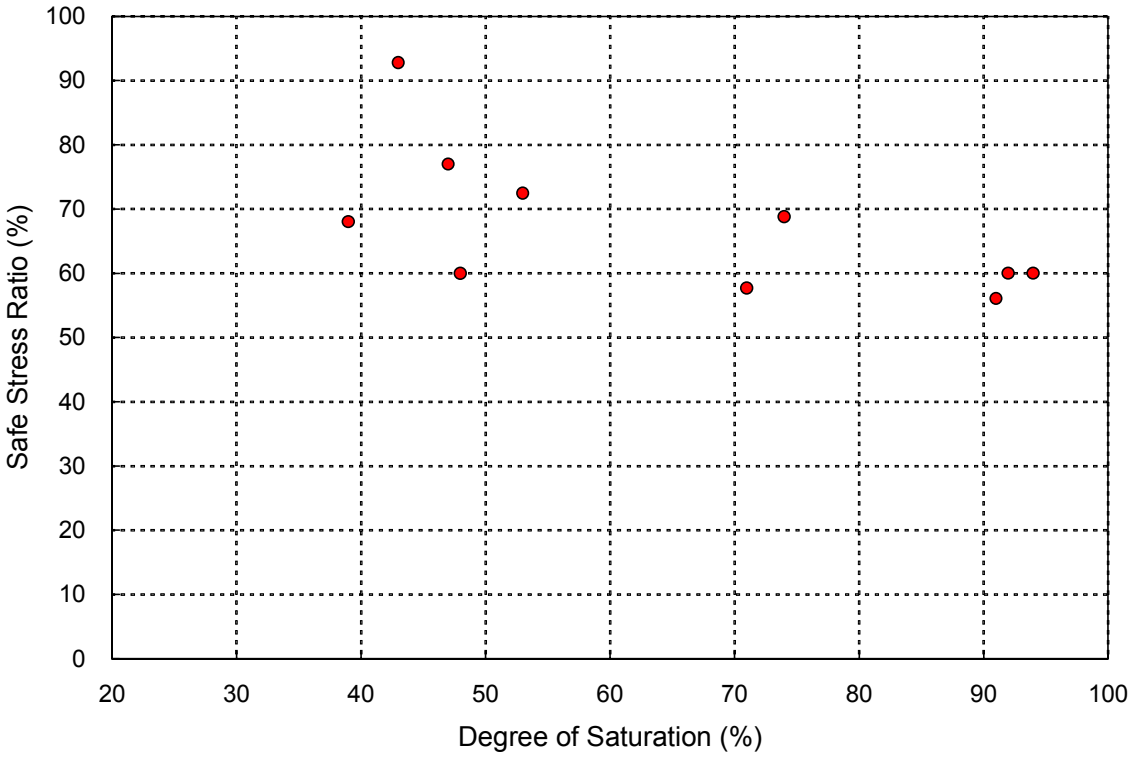

Figure 21. Effect of the degree of saturation on the stress ration level at which unstable permanent deformation occurs.

$$PD = mN + \frac{cN}{\left[1 + \left(\frac{cN}{a}\right)^{b}\right]^{1/b}} \quad \textbf{(8)}$$

$$PD = mN + a\left(1 - e^{-bN}\right) \quad \textbf{(9)}$$

$$PD = qe^{rN} - pe^{-sN} - q + p \quad \textbf{(10)}$$

Where PD = permanent deformation (mm),
N = number of load repetitions
all other letters represent regression coefficients

Once the coefficients of the regression models relating the permanent deformation to the number of load repetitions were known for each dynamic triaxial test, the number of load repetitions required to induce certain levels of plastic strain in the test samples could be solved. The plastic strain of the samples was calculated from the permanent deformation and original dimensions of the samples. The dynamic tests for a specific combination of material type, relative density, and degree of saturation were performed at various stress ratio levels, thus making it possible to study the relationship between the number of load repetitions (N) required to induce various levels of plastic strain and the stress condition (S) at which these load repetitions are applied.

The stress parameter that was used by Theyse to represent the shear stress condition is similar to the stress ratio used by Maree. The stress ratio, SR may be formulated in terms of deviator stress as given by Equation 11 or major principal stress as given by Equation 12. These two formulations result in slightly different calculated values of the stress ratio, however, these differences are of little practical consequence. The theoretical maximum value of the stress ratio is 1 when the applied shear stress equals the shear strength of the material. In practice, however, it is possible to do repeated load tests at stress ratios even slightly above 1, if the duration of the load pulses is kept short. The same numeric value for the stress ratio may also be generated at different absolute stress values, as illustrated in Figure 22. The stress ratio is used as the stress parameter in the discussions that follows in this section of the report.

$$SR = \frac{\sigma_1^a - \sigma_3}{\sigma_1^m - \sigma_3}$$

$$= \frac{\sigma_1^a - \sigma_3}{\sigma_3\left(\tan^2\left(45^\circ + \frac{\varphi}{2}\right) - 1\right) + 2C\tan\left(45^\circ + \frac{\varphi}{2}\right)} \quad \textbf{(11)}$$

$$SR' = \frac{\sigma_1^a}{\sigma_1^m}$$

$$= \frac{\sigma_1^a - \sigma_3}{\sigma_3\tan^2\left(45^\circ + \frac{\varphi}{2}\right) + 2C\tan\left(45^\circ + \frac{\varphi}{2}\right)} \quad \textbf{(12)}$$

Where:

σ	=	principal stress (kPa)
τ	=	shear stress (kPa)
φ	=	internal friction angle (°)
C	=	cohesion (kPa)
σ_1^m	=	maximum allowable major principal stress (kPa) given C, φ and σ_3
σ_1^w, σ_1^a	=	working or applied major principal stress (kPa)
σ_3	=	minor principal stress or confining pressure for the triaxial test (kPa)

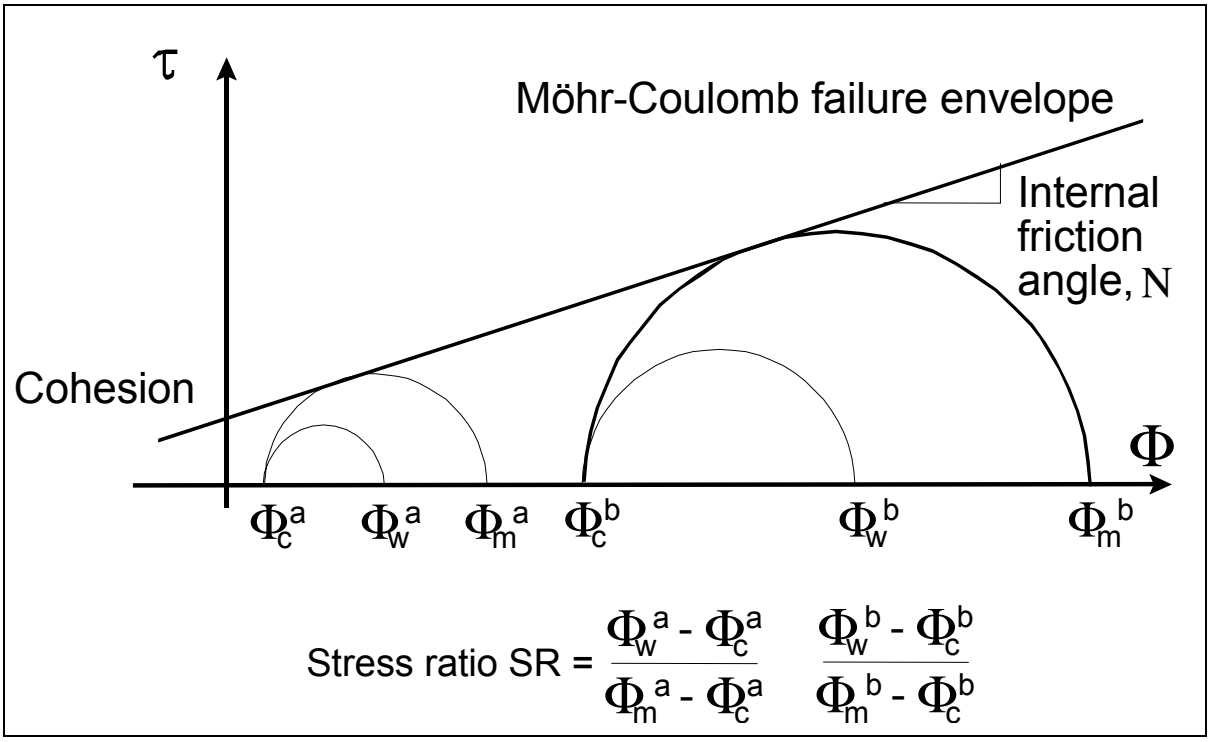

Figure 22. Equal values for the stress ratio generated at different values of absolute stress.

Figure 23 shows typical examples of S-N (stress ratio - N) data sets for three plastic strain levels (3, 7, and 13 percent) for crushed stone aggregate at 80.7 percent relative density (relative to apparent density) and at 33.4 and 78 percent saturation. The large influence of the degree of saturation on the number of load repetitions that can be sustained before a certain level of plastic strain is induced in the material, is evident from the data shown in Figure 23. Dynamic triaxial tests were also performed at 84.5 percent relative density and two levels of saturation to fully investigate the effect of relative density and degree of saturation on the number of load cycles that the crushed stone aggregate could sustain for different levels of plastic strain. The S-N data for the four possible combinations of relative density and degree of saturation at which tests were done were combined and a regression analysis was done for 3, 5, 7, 9 and 13 % plastic strain. The regression model is given in Equation 13 and Figure 24 contains contour plots of the model for different combinations of relative density and degree of saturation.

$$\log N = -13.43 + 0.29\,RD - 0.07\,S + 0.07\,PS - 0.02\,SR \qquad \textbf{(13)}$$

R^2 = 97.3 %; SEE = 0.313

Where: N = Number of load repetitions
RD = Relative density (%)
S = Degree of saturation (%)
PS = Plastic strain (%)
SR = Stress ratio (%)

4.4 Compaction Potential of Unbound Aggregate

The plastic strain model for a crushed stone aggregate presented in the previous section indicated that the density of unbound aggregate had a major influence on the plastic strain of the aggregate when subjected to repeated loading. This section presents a brief overview on the compaction potential of unbound aggregate from a study by Semmelink (*14*).

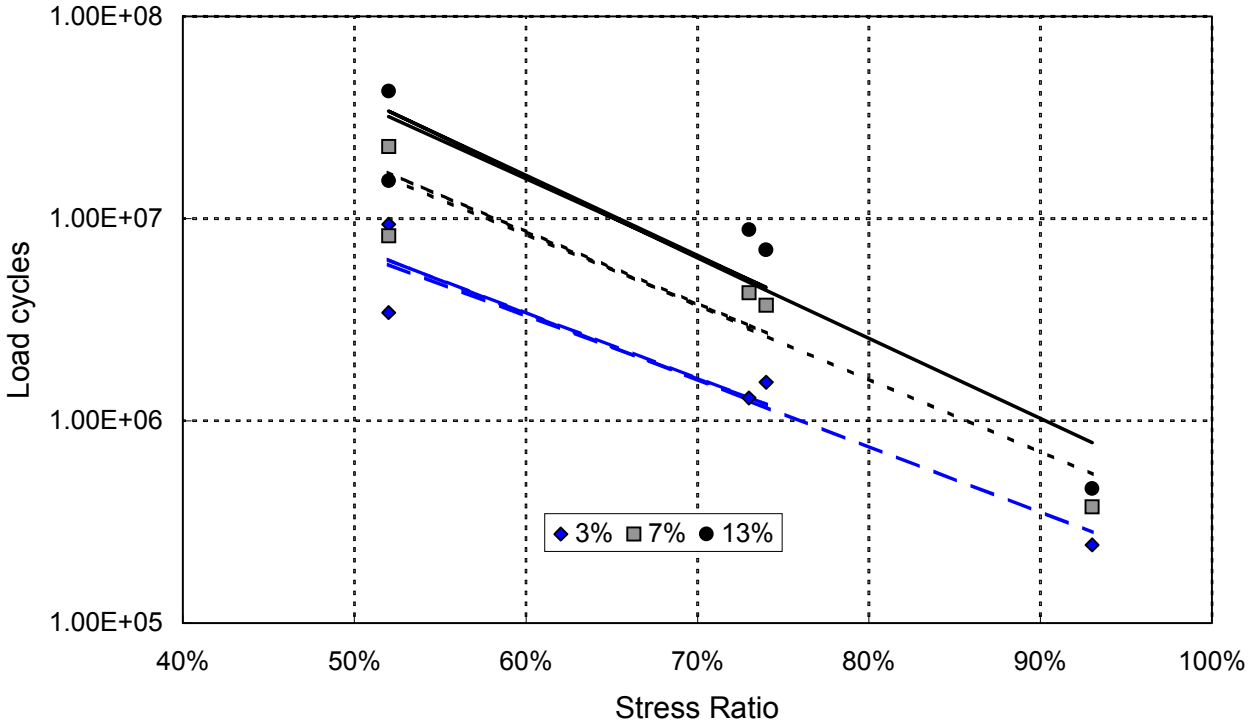

Figure 23a. Stress ratio – N data set for crushed stone aggregate, 80.7 percent relative density and 33.4 percent saturation.

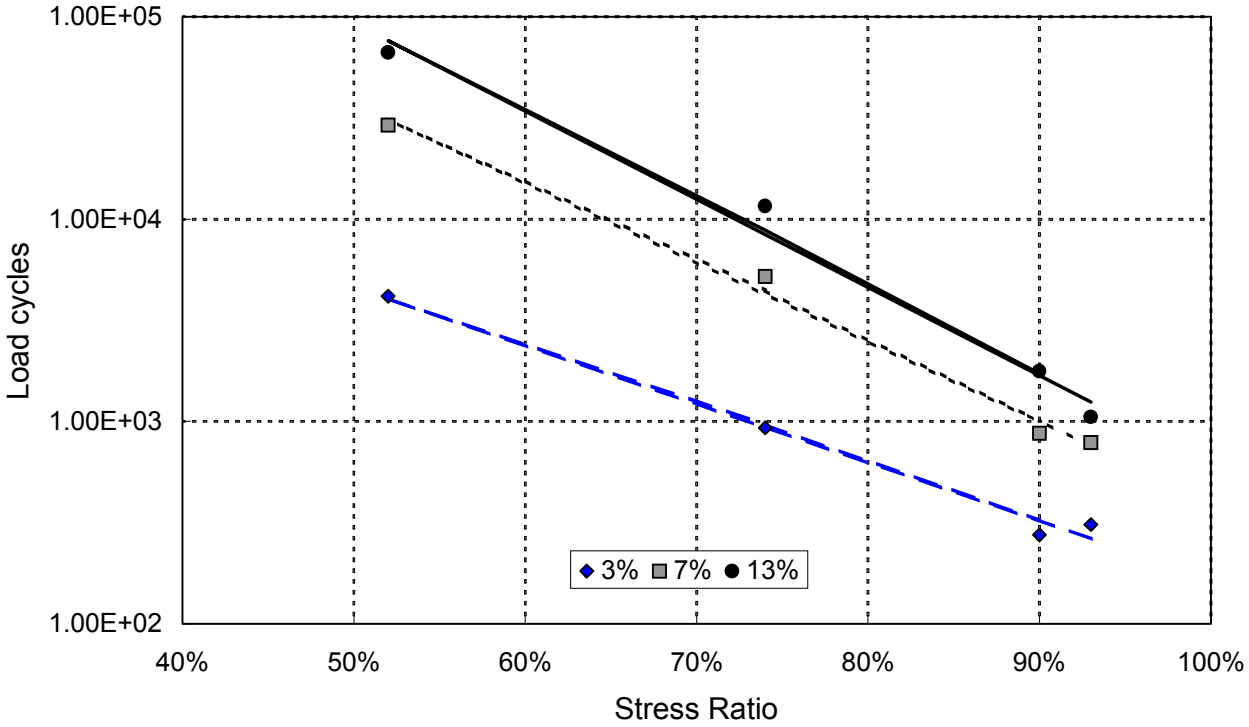

Figure 23b. Stress ratio – N data set for crushed stone aggregate, 80.7 percent relative density and 78 percent saturation.

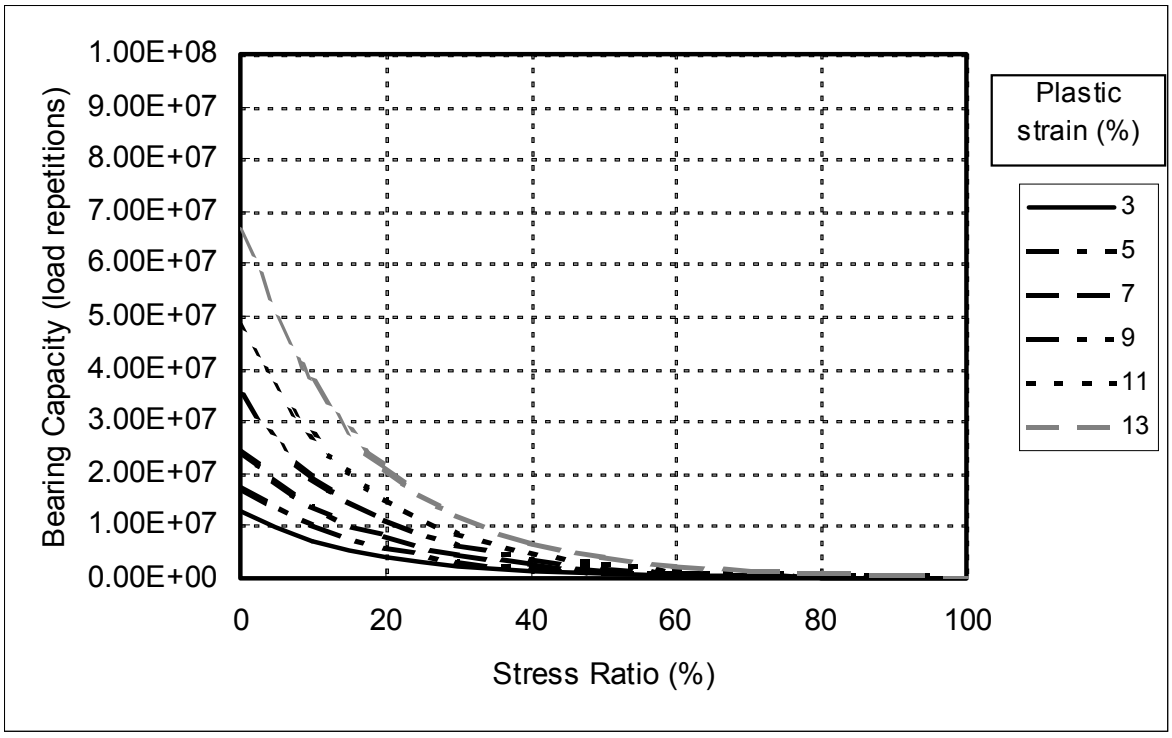

Figure 24a. Contour plot of the permanent deformation bearing capacity model for the unbound aggregate tested by Theyse, 86 percent relative density, 70 percent saturation.

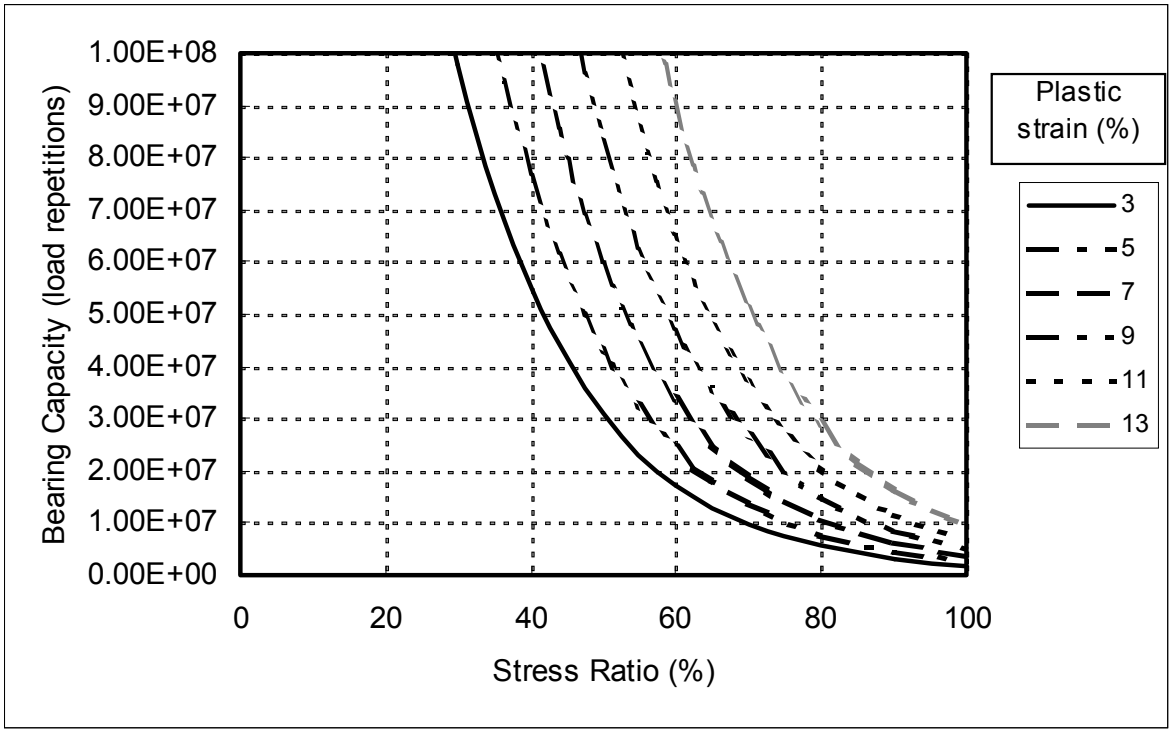

Figure 24b. Contour plot of the permanent deformation bearing capacity model for the unbound aggregate tested by Theyse, 86 percent relative density, 45 percent saturation.

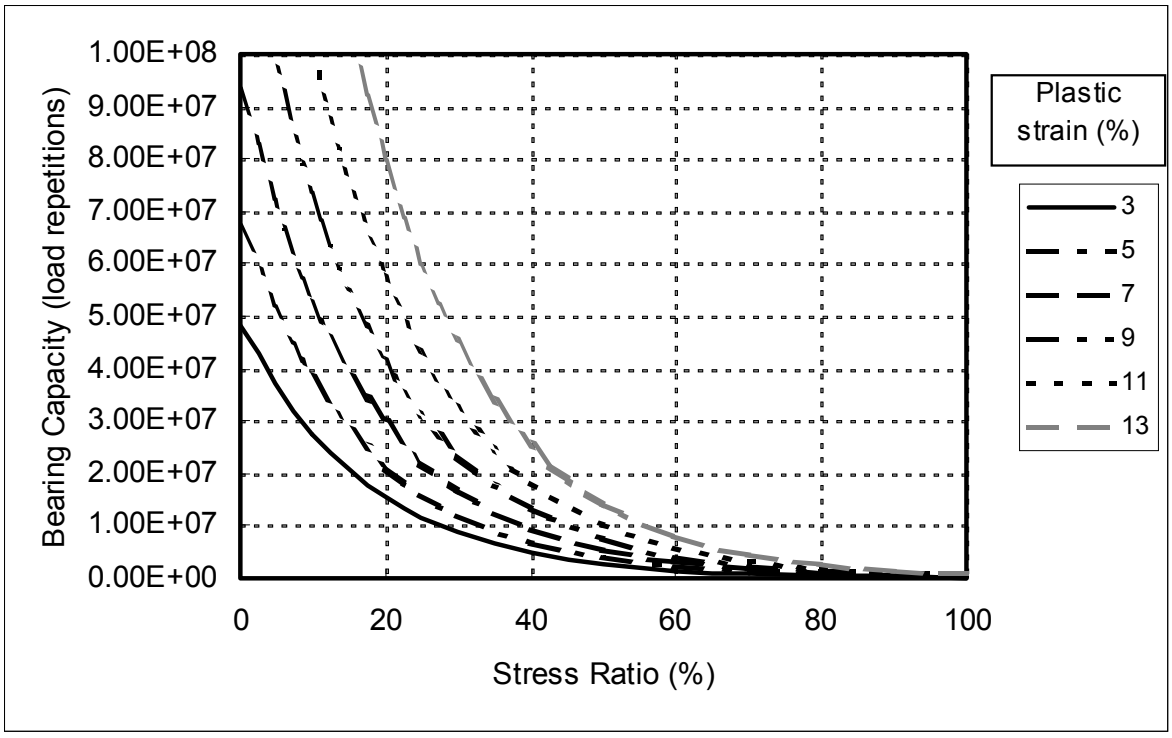

Figure 24c. Contour plot of the permanent deformation bearing capacity model for the unbound aggregate tested by Theyse, 88 percent relative density, 70 percent saturation.

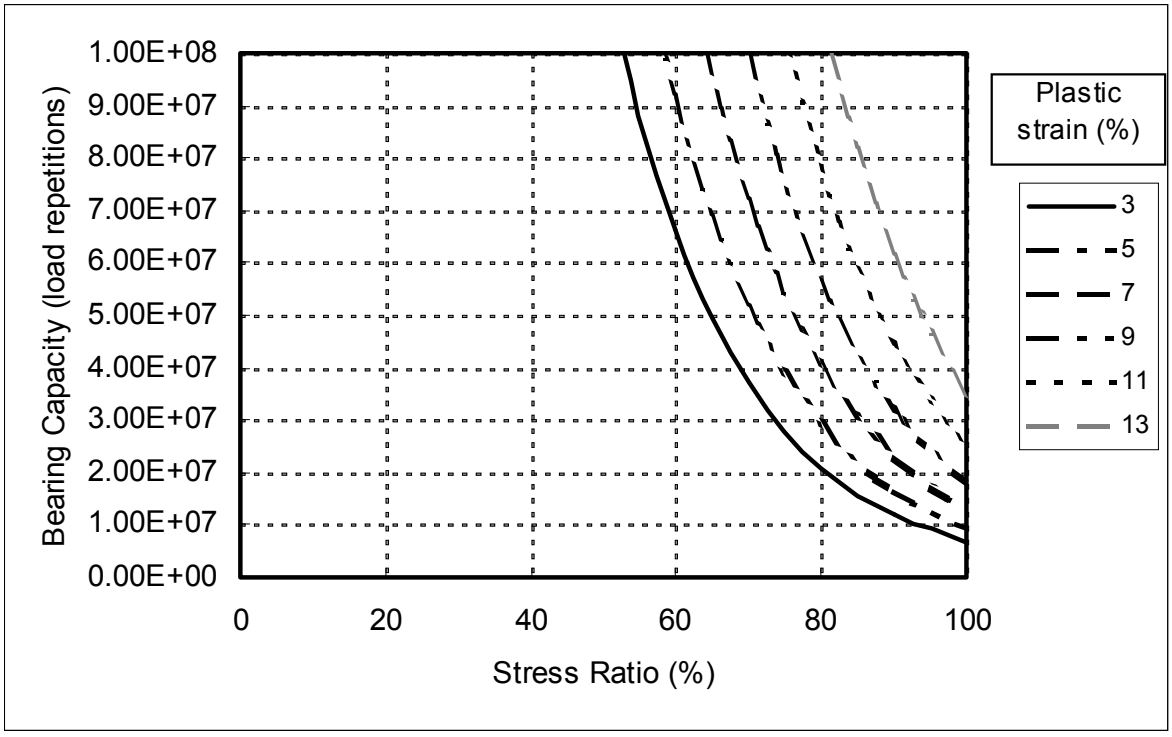

Figure 24d. Contour plot of the permanent deformation bearing capacity model for the unbound aggregate tested by Theyse, 88 percent relative density, 45 percent saturation.

The compaction potential is the expected practical maximum compaction that can be achieved for a given material. It is largely determined by the particle size distribution of the material. A higher density can be achieved with a continuously graded material than with a uniformly graded material of the same type. Semmelink therefore investigated the possibility of developing empirical predictive models for the maximum achievable density of an unbound aggregate, based on the particle size distribution of the material. The smallest sieve size used for routine grading analysis in South Africa is the 0.075 mm sieve. Instead of using the actual particle size distribution of the minus 0.075 mm fraction, which would have required hydrometer testing, in his models Semmelink used the liquid limit (LL) and linear shrinkage (LS) to characterize the minus 0.075 mm fraction material.

The approach followed by Semmelink deviates from that of Fuller and Talbot in the sense that they prescribe the requirements that the grading of the material has to meet in order to ensure that the maximum density is achieved. The grading of an aggregate from a natural source is, however, a given and it is not always possible or economically feasible to alter the grading. Semmelink therefore approached the problem with the aim of predicting the maximum achievable density for a given particle size distribution. The level of compaction that is achieved also depends on the compaction energy that is employed. Semmelink therefore developed models for modified AASHTO and vibratory table compaction effort. Each of these compaction methods has an optimum moisture content (OMC) associated with it. In addition to the density models, Semmlink also developed predictive models for estimating the optimum compaction moisture content for a given material and compaction effort.

The empirical models developed by Semmelink are:

$$MDD_{vib} = -39.34GF^{0.85} + 20.01C - 1.54LS - 11.05C^3 + 107.82$$

$$MDD_{mod} = -33.73GF^{0.85} + 19.28C - 1.21LS - 12.31C^3 + 99.94$$

$$OMC_{vib} = 23.14GF^{0.85} - 15.90C + 1.09LS + 11.16C^3 - 7.63$$

$$OMC_{mod} = 7.18GF^{0.85} + .035C - 0.55LS + 2.86C^3 + 0.80$$

Where:

C	=	(percentage passing the 0.425 mm sieve/100)/(LL/100)$^{0.1}$
GF	=	Σ(percentage passing a particular sieve size/nominal sieve size)/100 for the 75 mm, 63 mm, 53 mm, 37.5 mm, 26.5 mm, 19 mm, 13.2 mm, 4.75 mm, and 2 mm sieves
LS	=	linear shrinkage
LL	=	liquid limit

All of the above models had correlation coefficients higher that 90 percent and provide good estimates of the maximum achievable density of a material for which particle size distribution and Atterberg limits are known.

5.0 CONCLUSIONS AND RECOMMENDATIONS

Although the methods of specification for unbound granular material in South Africa and California differ, the basic materials seem to be similar for certain aggregate classes. The end product that is placed in a pavement layer is, however, expected to have different stiffness, strength, and performance levels because of the differences in specification. Data presented in this document illustrate the effect of the moisture content and density of an unbound material on the bearing strength of the material. The South Africa specification allows this to be taken into consideration when an unbound granular material is used in different pavement layers. The specification requires a higher density and bearing strength for layers closer to the pavement surface than for layers deeper down. The California specification does not incorporate the influence of density and moisture content on the bearing strength of the material. Furthermore, the California method for determining the reference density for compaction control effectively utilizes the wet density of the material. The following specific recommendations are therefore made regarding the California specification for the use of unbound granular material in pavements:

- The influence of density and moisture content on the bearing strength of the material should be incorporated in the specification. Bearing strength requirements for different pavement layers should be specified at specific density and moisture content levels.
- It is strongly recommended that the method for determining the reference density for compaction control should be changed to a method that utilizes dry density and that the compaction effort for the test should be increased above the currently required 95

percent relative to CTM 216, or a modified wet density such as in the Bureau of Reclamation manual (*18*).

As far as the effective stiffness of unbound granular material is concerned, HVS test results indicate that there is an increase in stiffness associated with an increase in the stress condition to which the unbound material is subjected. The correlation between resilient modulus and the bulk stress determined from the back-calculation of depth deflection results is, however, relatively poor although there is a general increase in resilient modulus as the bulk stress increases. There are several possible explanations for the relatively poor correlation. The bulk stress is calculated from linear elastic theory, which may lead to some error in the value of the bulk stress. The laboratory test results presented in this report indicate a strong dependency of the effective stiffness of unbound granular material on the density and moisture content of the material. These factors are often difficult to quantify for HVS tests and their effects on the back-calculated resilient modulus were not included in the correlation between the resilient modulus and bulk stress calculated from HVS data. The following parameters were identified as having an influence on the resilient response of unbound aggregate based on the HVS and laboratory data presented:

- **The dry density of the material expressed as a percentage of the solid density of the material.** The rate of change in the resilient modulus of unbound aggregate associated with a unit change in the relative dry density of the material is higher than the rate of change associated with changes in other parameters. The range of realistic values for the dry density of unbound aggregate is, however, limited to a range of values between about 78 and 88 percent of apparent density, thus limiting the overall effect on the resilient modulus.

- **The degree of saturation of the unbound aggregate.** The degree of saturation of the unbound material has a significant influence on the resilient modulus of the material. Realistic values for the degree of saturation can vary between 30 and 100 percent, thereby having a relatively large influence on the resilient response of the material.
- **The level of confinement of the unbound material.** An increase in the level of confinement of unbound aggregate causes the material to respond in a stiffening manner with an associated higher value for the resilient modulus of the material. The confinement may be quantified by the minor principal stress, the octahedral normal stress, or the bulk stress.
- **The shear stress imposed on the material.** In addition to the stress stiffening behavior of unbound material, there is also a reduction in stiffness as the shear strength of the material is approached. The imposed shear stress may be quantified by the deviator stress, the octahedral shear stress or the stress ratio.

The static shear strength of unbound aggregate is influenced by the relative dry density and degree of saturation of the material. The friction angle of crushed stone aggregate shows a general increase as the relative dry density increases and the cohesion decreases as the degree of saturation increases. There are, however, other factors that have an influence on the static shear strength parameters of the material, such as the particle size distribution and the characteristics of the course and fine particles in the material. Predictive models relating the shear strength parameters of unbound materials to the particle size distribution of the material and the characteristics of the course and fine aggregate particles should be investigated.

The permanent deformation of unbound granular material is affected by the following parameters:

- the relative dry density of the material;
- the degree of saturation of the material, and
- the combined level of confining and shear stress imposed on the material. This combined confining and shear stress condition is best represented by the stress ratio concept as defined in this report. The stress ratio is, in turn, determined by the shear strength parameters of the material, which depend on the relative dry density and degree of saturation of the material.

Predictive models for the permanent deformation bearing capacity of unbound aggregate incorporation the effect of relative dry density, degree of saturation, and stress ratio are presented in this report. These models were calibrated for specific aggregates with a relatively high degree of accuracy, but need to be extended to cover a wider range of materials used in California.

6.0 REFERENCES

1. California State Department of Transportation (Caltrans). *Caltrans Highway Design Manual.* Sacramento, California. November, 2001.

2. Caltrans. 1999. *Test Plan for CAL/APT Goal 5.* University of California at Berkeley Pavement Research Center, Transportek, and Dynatest Consulting, Inc.

3. Bejarano, M. O., J. T. Harvey, A. Ali, M. Russo, D. Mahama, D. Hung, and P. Preedonant. *Performance of Drained and Undrained Flexible Pavement Structures under Wet Conditions Accelerated Test Data Test Section 543–Drained.* Report prepared for California Department of Transportation by the University of California Pavement Research Center. August 2002.

4. Bejarano, M. O., J. T. Harvey, A. Ali, M. Russo, D. Mahama, D. Hung, and P. Preedonant. *Performance of Drained and Undrained Flexible Pavement Structures under Wet Conditions Accelerated Test Data Test Section 544–Undrained.* Report prepared for California Department of Transportation by the University of California Pavement Research Center. August 2002.

5. Bejarano, M. O., J. T. Harvey, A. Ali, M. Russo, D. Mahama, D. Hung, and P. Preedonant. *Performance of Drained and Undrained Flexible Pavement Structures under Wet Conditions Accelerated Test Data Test Section 545–Undrained.* Report prepared for California Department of Transportation by the University of California Pavement Research Center. August 2002.

6. Bejarano, M. O., J. T. Harvey, A. Ali, D. Mahama, D. Hung, and P. Preedonant. *Performance of Drained and Undrained Flexible Pavement Structures under Conditions of Saturated Base - Accelerated Pavement Testing Evaluation Goal 5 HVS.* Report prepared for California Department of Transportation by the University of California Pavement Research Center. August 2002.

7. Shackelton M C. 1995. *Modelling of the Permanent Deformation of Untreated Pavement Layers*. M Eng thesis, University of Pretoria, Republic of South Africa.

8. Maree, J H, van Zyl, N J W and Freeme, C R. 1982. "Effective Moduli and Stress Dependence of Pavement Materials as Measured in some Heavy Vehicle Simulator Tests." *Transportation Research Record 852*, Transportation Research Board, Washington D.C., pp. 52–60.

9. Wolff H. 1992. *Elasto-Plastic Behaviour of Granular Pavement Layers in South Africa.* Ph. D. thesis, University of Pretoria, Republic of South Africa.

10. Theyse H L. 1997. "Mechanistic Empirical Modelling of the Permanent Deformation of Unbound Pavement Layers." *Proceedings of the Eighth International Conference on the Structural Design of Asphalt Pavements.* Seattle, University of Washington, pp 1579–1594.

11. Van der Merwe, C J. 1988. *Some aspects of road subsurface drainage in South Africa*. Ph. D. thesis, University of Pretoria, Republic of South Africa.

12. Maree J H. 1982. *Aspekte van die Ontwerp en Gedrag van Padplaveisels met Korrelmateriaalkroonlae.* (*Aspects of the Design and Behavior of Road Pavements with Granular Base Layers*). Ph. D. thesis, University of Pretoria, Republic of South Africa.

13. Theyse, H L. 1999. *Laboratory Design Models for Materials Suited to Labour-intensive Construction*. Contract Report CR-99/038, Transportek, CSIR, Pretoria, Republic of South Africa.

14. Semmelink ,C J. 1991. *The Effect of Material Properties on the Compactability of Some Untreated Road-building Materials.* Ph. D. thesis, University of Pretoria, Republic of South Africa.

15. May, R W and Witczak, M W. 1981. "Effective granular modulus to model pavement response." *Transportation Research Record 810*, Transportation Research Board, Washington D.C., pp. 1–9.

16. Uzan, J. 1985. "Characterization of Granular Materials." *Transportation Research Record 1022*, Transportation Research Board, Washington D.C., pp. 52–59.

17. Maree J H. 1978. *Ontwerpparameters vir Klipslag in Plaveisels*. (*Design Aspects for Crushed Stone in Pavements*). M Eng. thesis, University of Pretoria, Republic of South Africa.

18. California State Department of Transportation (Caltrans). *Standard Specifications*. Sacramento, California. July 1999.

APPENDIX A: PAVEMENT AND INSTRUMENTATION DETAIL OF HVS TEST SECTIONS

HVS-section Nr: 303A2	Region: Macleantown, Eastern Cape	Road Nr: TR86	Year of test: 1986

Pavement structure

Instrumentation detail

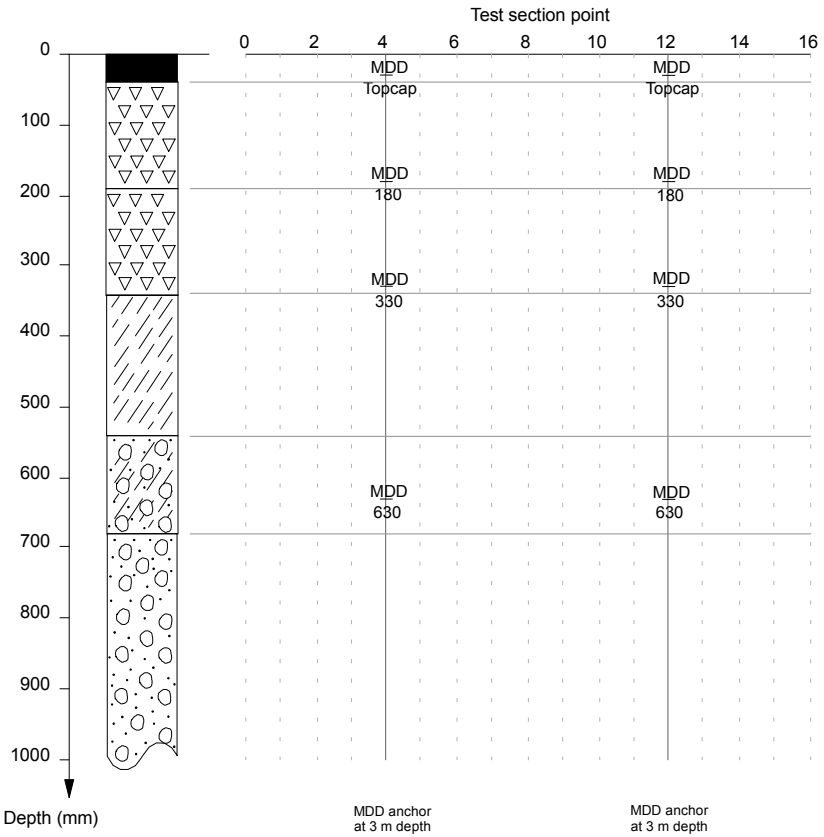

Pavement material information

Layer	Type	Material properties (UCS, CBR, MDD, OMC,etc)	Field Density (kg/cub m)	Field MC (%)	TRH14 class
0 - 40	Asphalt				
40 - 190	Crushed Stone	AD = 2658 kg/cub m mDD = 2198 (2204), OMC = 7,7 (7,6) CBR = 176 @ 98 % GM = 2,56	2149,6 (2153,3) 80,8% AD	4,4 (2,1)	G2/G3
190 - 340	Crushed stone drainage layer	AD = 2643 kg/cub m mDD = 2027 (2077), OMC = 9,9 (10,8) CBR = 52 @ 95 % GM = 2,67	2025,0 (2037,5) 76,6% AD	2,8 (2,6)	G5
340 - 540	Lime stabilized upper selected	Decomposed Dolorite, 4% lime mDD = 2165 (2070), OMC = 10,4 (6,5) CBR = 82 @ 93 % GM = 2,32	2158,5 (1993,4)	8,1 (8,5)	C4
540 - 680	Lime modified lower selected	Decomposed Dolorite, 1,5% lime mDD = 2278 (2064), OMC = 8,0 (10,7) CBR = 27 @ 93 % GM = 2,36	2241,5 (1964,9)	7,1 (7,6)	C5
680 +	In-situ subgrade	mDD = 2197, OMC = 7,9 CBR = 31 @ 93 % GM = 2,03			G6

Data in brackets were collected during 1998, original (1986) data shown outside brackets

Load sequence detail:

Repetitions		Test information		
From	To	Wheel load	Tyre pressure	Water added
0	411 413	100 kN	690 kPa	No
411 413	531 896	40 kN	520 kPa	Yes

Related reports:

van der Merwe C J, Horak E. 1986. *East London HVS experimental sections: Objectives and preliminary investigation.* National Institute of Transport and Road Research (NITRR), CSIR. (Technical Note TPC/1/86)

van der Merwe C J, de Villiers E M, Horak E. 1987. *HVS aided evaluation of a drainable subbase layer in the Eastern Cape.* NITRR, CSIR. (Research Report RR486)

HVS-section Nr: 332A2	Region: Port Elizabeth, Eastern Cape	Road Nr: N2/11	Year of test: 1988

Pavement structure

Instrumentation detail

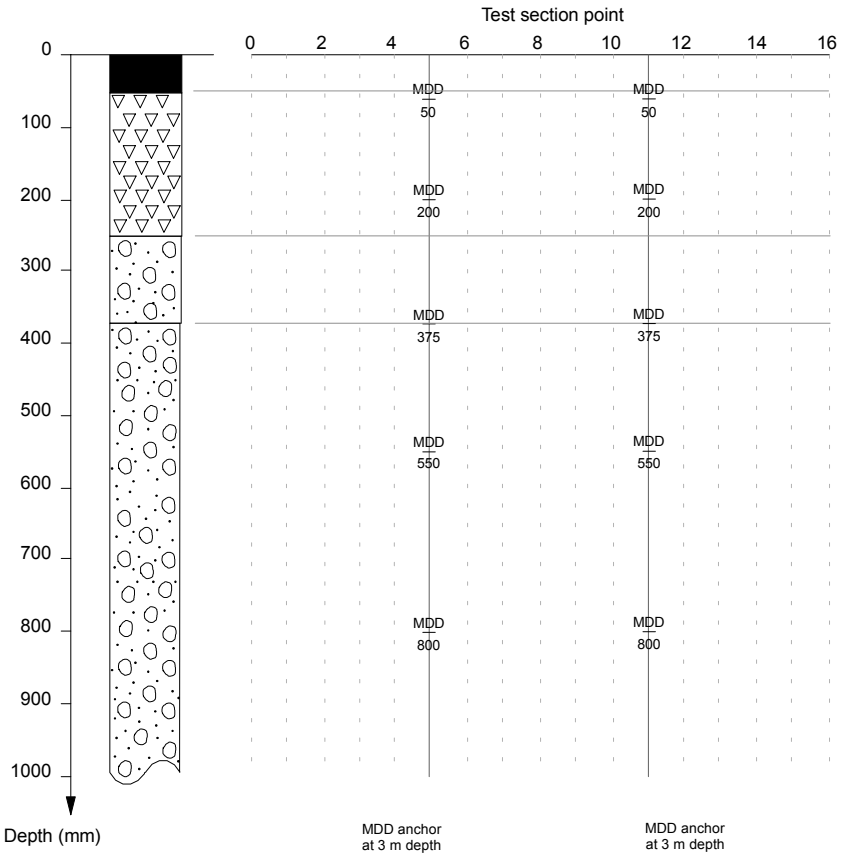

Pavement material information

Layer	Type	Material properties (UCS, CBR, MDD, OMC,etc)	Field Density (kg/cub m)	Field MC (%)	TRH14 class
0 - 50	Asphalt	New and old asphalt surfacing layers			
50 - 250	Crushed Stone	AD = ???? kg/cub m mDD = 2233, OMC = 5,5 CBR = 91 @ 98 % GM = 2,25	99,5% mDD	3,1	G2
250 - 370	Natural gravel subbase	mDD = 1908, OMC = 10,3 CBR = 48 @ 95 % GM = 2,06	87,4% mDD	12,9	G5
370 +	In-situ subgrade	Stony limestone and sand mDD = 1926 OMC = 12,1 CBR = 27 @ 93 % GM = 1,65	95,8% mDD	11,2	G6

Load sequence detail:

Repetitions		Test information		
From	To	Wheel load	Tyre pressure	Water added
0	604 735	40 kN	520 kPa	No
604 735	1 245 733	60 kN	690 kPa	No

Related reports:

No report available

HVS-section Nr: 341A2a	Region: Richmond, Central Cape	Road Nr: TR9-7 (N1)	Year of test: 1988

Pavement structure

Instrumentation detail

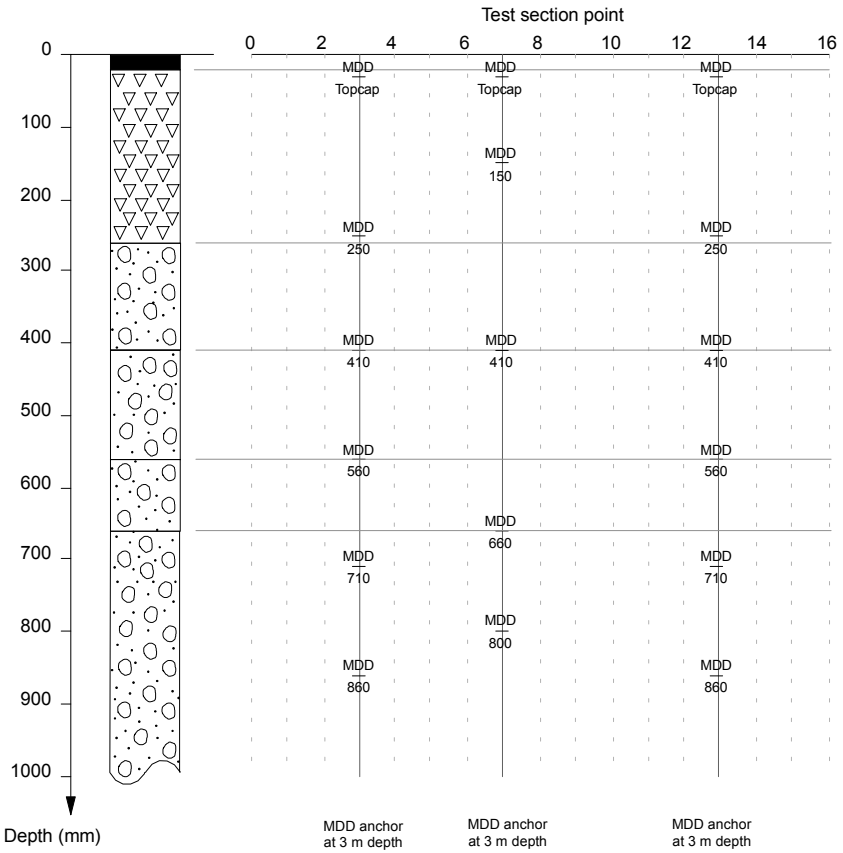

Pavement material information

Layer	Type	Material properties (UCS, CBR, MDD, OMC,etc)	Field Density (kg/cub m)	Field MC (%)	TRH14 class
0 - 20	Seal	Double seal (13,2 and 7,6 mm)			
20 - 260	Crushed stone base	AD = 2910 kg/cub m mDD = 2372, OMC = 5,2 CBR = 91 @ 98 % GM = 2,53	81 to 84 % AD 101 - 103 % mDD		G2
260 - 410	Natural gravel subbase	mDD = 1904, OMC = 11,3 CBR = 85 (56 % @ 95%) GM = 2,22	98 % mDD		G5
410 - 560	Natural gravel upper selected subgrade	mDD = 1891 OMC = 12,1 CBR = 49 (21 % @ 93 %) GM = 1,58	97 % mDD		G7
560 - 660	Natural gravel lower selected subgrade	mDD = 1956, OMC = 10,9 CBR = 51 (14 % @ 93 %) GM = 1,45	95 % mDD		G8
660 +	In-situ subgrade	mDD = 2004, OMC = 10,9 CBR = 16	96 % mDD		G8

Data in brackets were calculated from construction results, other data from reports listed below

Load sequence detail:

Repetitions		Test information		
From	To	Wheel load	Tyre pressure	Water added
0	250 834	40 kN	520 kPa	No
250 834	449 333	60 kN	690 kPa	No
449 333	703 600	80 kN	690 kPa	No
703 600	1 285 568	100 kN	690 kPa	No

Related reports:

Nienaber C J. 1988. *Planning of the HVS test on Road TR9-7 (N1) between Three Sisters and Richmond.* (In afrikaans) Division for Roads and Transport Technology, CSIR. (I/FP/19/88)

Du Doit G J. 1988. *Interim report on the behaviour of crushed stone base layers - Report on the HVS test at Richmond-Three Sisters (Road TR9-7).* (In afrikaans) Division for Roads and Transport Technology, CSIR. (I/FP/37/88)

HVS-section Nr: 327A3	Region: Umkomaas, KwaZulu-Natal	Road Nr: N2 - 23	Year of test: 1988

Pavement structure

Instrumentation detail

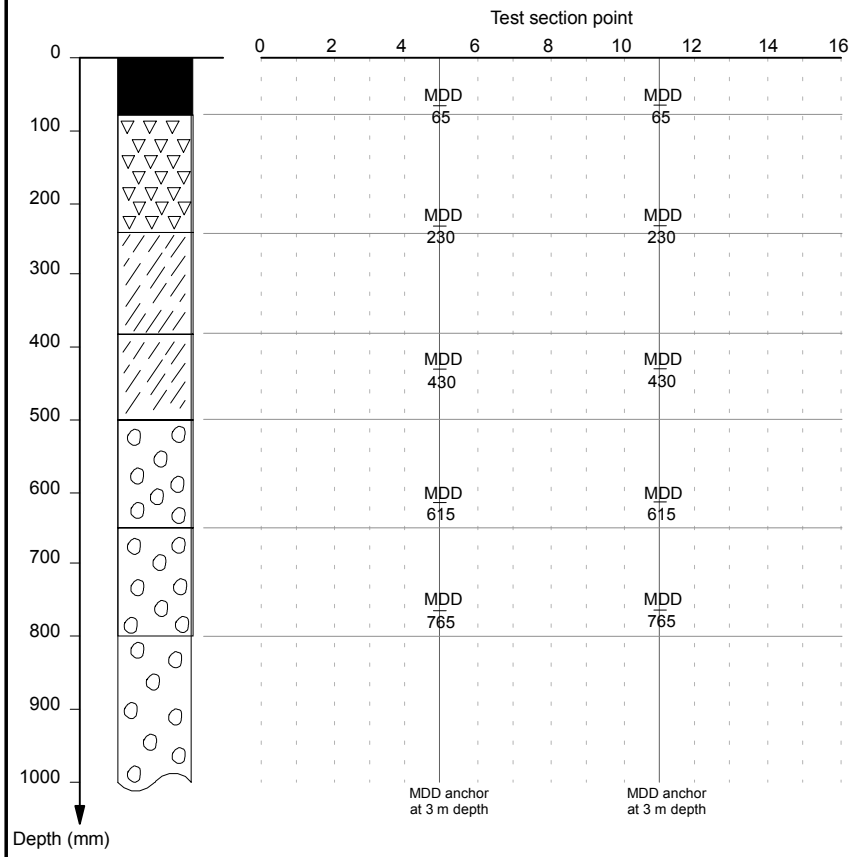

Pavement material information

Layer	Type	Material properties (UCS, CBR, MDD, OMC,etc)	Field Density (kg/cub m)	Field MC (%)	TRH14 class
0 - 80	Asphalt	50 mm AS, 30 mm AC Flow = 3,9 mm Stability = 4,1 kN	2260 (b) 2275 (a)		
80 - 240	Crushed Stone	AD = 2696 kg/cub m mDD = 2260, OMC = 6,2 CBR = 128 @ 98 % GM = 2,5	2280 (b) 2370 (a) 2209	2,9	G1
240 - 380	Cement-treated crushed stone	mDD = 2158, OMC = 8,1 CBR = 127 @ 95 % GM = 2,4	2070 (b) 2110 (a) 2024	6,6	C3
380 - 500	Lime stabilized gravel	mDD = 1978, OMC = 11,3 CBR = 68 @ 95 % GM = 2,3	2110 (b) 2140 (a) 2017	8,1	C4
500 - 650	Selected subgrade	mDD = 2031, OMC = 9,0 CBR = 31 @ 93 % GM = 2,0	2010 (b) 2055 (a) 1835	8,6	G6
650 - 800	In-situ subgrade	mDD = 2058, OMC = 8,7 CBR = 31 @ 93 % GM = 1,6	2015 (b) 2040 (a) 1835	8,6	G6
800 +	In-situ subgrade				

Load sequence detail:

Repetitions		Test information		
From	To	Wheel load	Tyre pressure	Water added
0	708 000	100 kN	690 kPa	No
708 000	1 069 000	40 kN	520 kPa	Yes, points 0 - 8
1 069 000	1 669 000	100 kN	690 kPa	Yes, points 0 - 8

Related reports:

Wright, B G and Horak E. 1988. *Report on the crushed stone section at Umgababa in Natal.* Division of Roads and Transport Technology, CSIR. (Unpublished report.)

HVS-section Nr: 398A4	Region: Cullinan, Gauteng	Road Nr: Road 2388	Year of test: 1997

Pavement structure

Instrumentation detail

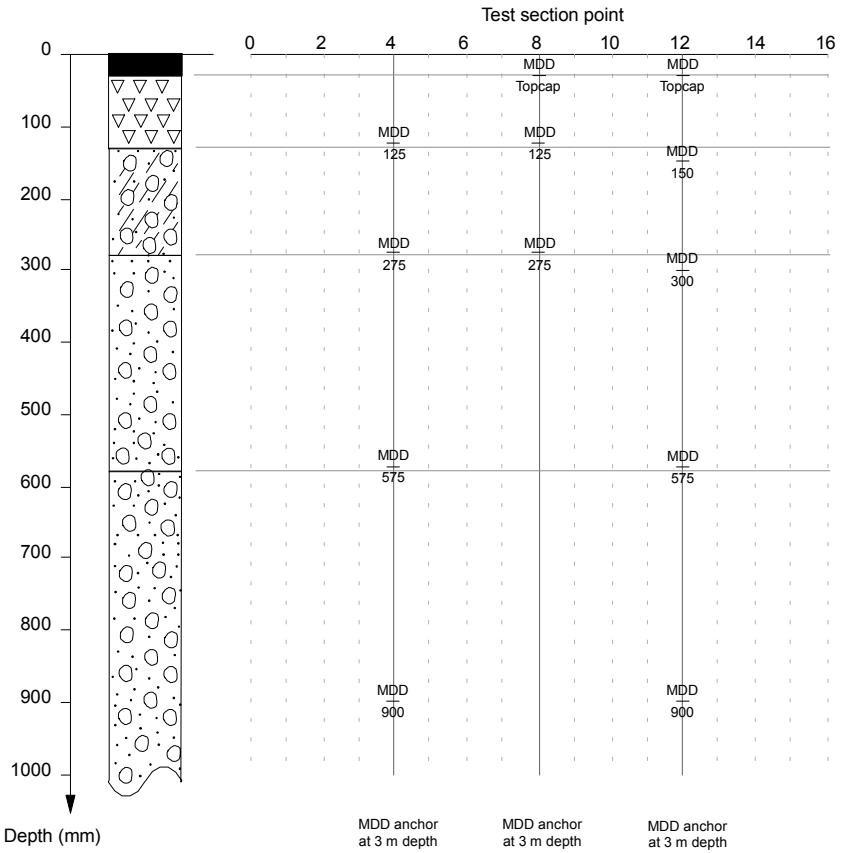

Pavement material information

Layer	Type	Material properties (UCS, CBR, MDD, OMC,etc)	Field		TRH14 class
			Density (kg/cub m)	MC (%)	
0 - 30	Asphalt	Fine continuous correction layer and medium continuous wearing course 5% NATREF 60/70 B12 binder Rice density = 2454 kg/cub m	2318 5,5 % voids		AC
30 - 130	Crushed stone base	AD = 2664 kg/cub m, BD = 2565 kg/cub m mDD =2188, OFC = 7,5 CBR = 111 @ 98% GM = 2,3 PI = Non-plastic	2149 98 % mDD	3,5	G3
130 - 280	Cement-treated gravel subbase	Sandstone conglomerate, 2,5% OPC reworked with 1,5% OPC mDD = 2154, OMC = 6,7 UCS @ 100 = 2486 @ 97 = 1940 GM = 2,2 PI = Non-plastic	2171 101 % mDD	2,8	C3
280 - 580	Natural gravel selected subgrade	Sandstone conglomerate mDD = 2155, OMC = 7,1 CBR = 21 @ 93 % GM = 2,2 PI = Non-plastic	2204 102 % mDD	6,0	G7
580 +	Natural gravel fill	Sandstone conglomerate mDD = 2155, OMC = 7,1 CBR = 21 @ 93 % GM = 2,2 PI =Non-plastic			G7

Load sequence detail:

Repetitions		Test information		
From	To	Wheel load	Tyre pressure	Water added
0	200 000	40 kN	520 kPa	No
200 000	400 000	70 kN	670 kPa	No
400 000	536 653	70 kN	670 kPa	Yes

Related reports:

Theyse H L. 1997. *The construction of the HVS experimental sections on Road 2388 near Cullinan.* Transportek, CSIR. (Confidential Contract Report CR-97/071)

Theyse H L. 1999. *Laboratory design models for materials suited to labour-intensive construction.* Transportek, CSIR. (Confidential Contract Report CR-99/038)